A Concise Model and Analysis for Heat-Induced Withdrawal Reflex Caused by Millimeter Wave Radiation

Hongyun Wang[1], Wesley A. Burgei[2], Hong Zhou[3*]

[1]Department of Applied Mathematics, University of California, Santa Cruz, USA
[2]U.S. Department of Defense, Joint Non-Lethal Weapons Directorate, Quantico, USA
[3]Department of Applied Mathematics, Naval Postgraduate School, Monterey, CA, USA
Email: *hzhou@nps.edu

Abstract

In this study, we consider the heat-induced withdrawal reflex caused by exposure to an electromagnetic beam. We propose a concise dose-response relation for predicting the occurrence of withdrawal reflex from a given spatial temperature profile. Our model is distilled from sub-step components in the ADT CHEETEH-E model developed at the Institute for Defense Analyses. Our model has only two parameters: the activation temperature of nociceptors and the critical threshold on the activated volume. When the spatial temperature profile is measurable, the two parameters can be determined from test data. We connect this dose-response relation to a temperature evolution model for electromagnetic heating. The resulting composite model governs the process from the electromagnetic beam deposited on the skin to the binary outcome of subject's reflex response. We carry out non-dimensionalization in the time evolution model. The temperature solution of the non-dimensional system is the product of the applied power density and a parameter-free function. The effects of physical parameters are contained in non-dimensional time and depth. Scaling the physical temperature distribution into a parameter-free function greatly simplifies the analytical solution, and helps to pinpoint the effects of beam spot area and applied power density. With this formulation, we study the theoretical behaviors of the system, including the time of reflex, effect of heat conduction, biological latency in observed reflex, energy consumption by the time of reflex, and the strategy of selecting test conditions in experiments for the purpose of inferring model parameters from test data.

Keywords

Millimeter Wave Radiation, Heat-Induced Pain, Withdrawal Reflex,

Dose-Response Model, Biological Latency, Non-Dimensionalization, Effect of Heat Conduction

1. Introduction

Millimeter wave (MMW) is a subset of radio frequency (RF) in the 30 - 300 gigahertz (GHz) range. Human body exposure to MMW radiation at sufficiently high intensities increases the skin temperature and induces thermal pain. Since the energy penetration depth of MMW irradiation in tissue is very shallow (millimeter or less), the primary effect of MMW exposure is temperature increase near the skin surface. Due to the rapid growth in using MMW in common applications including wireless communications systems, automobile collision avoidance systems, airport security screening, non-lethal crowd control weapons, medical imaging, and detection of vital signs such as respiration and heartbeat rates [1] [2] [3], it is important to understand the thermal responses of humans to MMW irradiation and to evaluate biological safety with respect to thermal hazards.

Considerable work has been done in MMW interactions with the human body [4]. We briefly review a few papers that motivate us for this study. In [5], cutaneous thresholds for thermal pain were measured in 10 human subjects (3 female and 7 male Caucasian volunteers, 31 - 70 years old with an average age of 43.7, military or DoD civilians or contractors). Each subject was tested with 3-second exposures to 94 GHz electromagnetic wave of intensity up to 1.8 W/cm². During each exposure, the temperature increase at the skin's surface was measured by infrared thermography. The mean baseline temperature of the skin was 34°C. The irradiated area of the skin has a diameter of 4 cm. The threshold for pricking pain was 43.9°C (at skin surface). The measured surface temperature was in good agreement with a simple one-dimensional thermal model that accounted for heat conduction and for the penetration depth of the electromagnetic energy into tissue. One important observation in [5] was that the skin surface temperature increased roughly by 10°C after a 3-second exposure to 1.8 W/cm² at 94 GHz.

Heating of tissues by electromagnetic waves has also been studied in [6] using Pennes' bioheat equation, which includes the effect of the blood convection in dissipating the heat. The model was used to estimate the threshold for perception of pain as a function of frequency and exposure duration in the case of plane-wave irradiation. The numerical results in [6] agree well with the experimental thresholds for warmth perception evoked by electromagnetic waves of 2.45 - 94 GHz applied to the back of the test subject for 10-second intervals.

In [7] [8], a one-dimensional multi-layer tissue model was used and solved with the finite difference method to predict temperature variations in the skin exposed to electromagnetic waves. This approach allows estimation of tempera-

ture distribution and prediction of burn injury in different layers of the skin depending on blood perfusion rate, thermal conductivity, power density, and exposure time. Even though the numerical simulations were focused on electromagnetic waves with frequencies of 10 GHz and below, this multi-layer model can be extended directly to MMW frequencies. These studies concluded that the rate of skin surface temperature increase in humans in response to brief, high-power MMW exposures can be mathematically modeled using the one-dimensional thermal conduction model.

In [9], a spherical heterogeneous model was developed to simulate the thermal effects (surface and subsurface) on a primate (monkey) head exposed to far-field radiation at 100 GHz. It was found that temperature (both surface and subsurface) increases as the energy level increases, whereas high-power millimeter-waves (HPMs) with power densities in the range of 1.0 to 3.0 W/cm^2 for 3 seconds have a higher peak temperature than low-power millimeter-waves (LPMs) in the range of 0.1 to 0.3 W/cm^2 for 30 seconds. The surface temperature increase is generally linear with applied energy density for HPMs except under combined conditions of high blood-flow rate and high-energy density. In contrast, with LPMs, the surface temperatures do not behave linearly with respect to incident energy. The simulations also showed that the subsurface (*i.e.*, mid-scalp and mid-skull) temperature increases are substantially damped compared to the surface (*i.e.*, scalp) temperature.

Far-field exposure of the human face to a linearly polarized plane wave at frequencies from 6 to 100 GHz and with exposure durations of 100 milliseconds to 10 seconds was modeled in [10]. The Maxwell equations were solved using a finite-difference time-domain solver. The Pennes' bioheat transfer equation extended with a term representing the electromagnetic power absorption was used to model body temperature and it was numerically solved. The electromagnetic and thermal simulations revealed highly non-uniform frequency-dependent patterns of temperature rise.

According to a review published in 2016 [11], there are very limited data in the literature related to skin temperature rises or thermal sensation thresholds in humans exposed to MMWs. Most data involves brief exposures to MMWs around 94 GHz [12]. For example, experiments with 13 male adults were conducted in San Antonio, TX to quantify the thermal and behavioral effects of exposure to 30 kW and 95 GHz MMW [13]. The experimental results indicated that the power density necessary to achieve pain intolearability in 90% of the human subject population is 3.03 W/cm^2 when the duration of the exposures was fixed at 3 seconds. The effects of variable spot size (beam diameter) on human exposure to 95 GHz MMW were investigated in [14] with a small number of volunteers. The experiments confirmed that repel times of stationary subjects decreased with increasing beam size, although the strength of this relationship varied with power density.

In this paper, we study the mathematical framework for human subjects' behavioral responses when exposed to millimeter wave radiation. The electromag-

netic energy absorbed in the skin increases the skin temperature via dielectric heating. High temperature activates the heat-sensitive nociceptors which produce a stimulus that is sent to the Central Nervous System (CNS) [15]. When the stimulus is sufficiently strong, the withdrawal reflex is initiated and the subject moves away from the exposure. The withdrawal reflex is also called nociceptive flexion reflex and is a spinal reflex intended to protect the body from noxious stimulations [16]. In the ADT CHEETEH-E model [17] recently developed at the Institute for Defense Analyses, the process from the power emitted at the radiation antenna to the subject's behavioral response is divided into multiple sub-steps, and model components were proposed to describe individual sub-steps [17]. In this study, we follow these model components as general guidelines and use only the physical principles of these model components. We construct a concise dose-response relation for predicting the occurrence of withdrawal reflex based on the spatial temperature profile. The resulting concise model is independent of the specific function forms and parameters used in the sub-steps of ADT CHEETEH-E [17]. In our formulation, the dose quantity is defined as the volume of activated region where the temperature is above the activation temperature of nociceptors. The dose-response model for withdrawal reflex is specified by only two parameters: the activation temperature of nociceptors (T_{act}) and the critical threshold on the dose quantity (z_c). When the spatial temperature profile at reflex is measurable, the two model parameters T_{act} and z_c can be determined from test data. The inference formulation for calculating T_{act} and z_c is based solely on the measured temperature profiles. It does not depend on any symmetry of temperature profile or electromagnetic heating or heat conduction. It does not require any input parameter.

The dose-response model maps a given spatial temperature profile to the binary outcome of subject's reflex response. We connect it to a time evolution model governing the temperature increase for electromagnetic heating in the skin. The result is a composite model that takes as input the electromagnetic beam deposited on the skin, which is characterized by the beam spot area and the power density. For the temperature evolution, we first consider the simple case of uniform temperature over beam cross-section with no heat conduction (which we shall call idealized case A). The exact solution of temperature is proportional to the time and proportional to the applied power density. Its spatial shape is determined by that of the electromagnetic heating. In order to assess the validity of no-conduction approximation, we consider the case of uniform temperature over the beam cross-section with heat conduction in the depth direction (which we shall call idealized case B). To pinpoint the effects of individual parameters and to facilitate the exact solution, we carry out non-dimensionalization. The temperature solution of the non-dimensional system is the product of the applied power density and a standardized parameter-free function, which we shall call the normalized temperature. The normalized temperature as a function of non-dimensional time and depth has no dependence on the power density or any other parame-

ters. The effects of physical parameters are contained in the non-dimensional variables and in the non-dimensional power density (the multiplier coefficient). Comparing the solutions, respectively, in the presence and in the absence of heat conduction, we find that the no-conduction approximation is appropriate only in the region away from the skin surface and only over a short time. With the analytical solution, we explore the theoretical behaviors of the system and discuss the issues listed below.

- We derive the asymptotic expansion of reflex time at large beam spot area, and compare the result with that in the case of no heat conduction.
- We investigate the biological latency (time delay) in the observed withdrawal reflex. We formulate an algorithm for determining the time delay in the observed withdrawal reflex. The algorithm is based solely on three data points of observed reflex time vs. applied power density. The algorithm is parameter-free, and thus, is operationally applicable in all situations.
- We carry out asymptotic analysis on the normalized temperature respectively for small time and for large time. Building on the asymptotic behaviors of normalized temperature, we construct asymptotic approximations of the reflex time respectively for large and for small applied power density.
- Using the asymptotic results obtained, we examine the energy consumption by the time of reflex, as a function of applied power density. We find that the energy consumption attains a minimum at a moderately large value of applied power density.
- We examine the spatial temperature profile at reflex and demonstrate that it converges to the no-conduction solution at large power density.
- We study how to select test conditions for determining model parameters $\left(T_{\mathrm{act}}, z_c\right)$ from the measured temperature profiles at reflex. Each data set yields only one constraint on $\left(T_{\mathrm{act}}, z_c\right)$. To determine both T_{act} and z_c simultaneously, we need to obtain distinct constraints on $\left(T_{\mathrm{act}}, z_c\right)$, which is achieved by carrying out tests both with large beam spot area and with moderate beam spot area.

Finally, we do a case study of Gaussian beams using numerical simulations. We revisit the theoretically predicted behaviors of the system derived in the idealized case B (uniform temperature over beam cross-section). For Gaussian beams (which do not satisfy the assumptions of case B), 1) we evaluate the performance of the algorithm for estimating the biological latency from a sequence of observed reflex times; 2) we examine the existence of energy consumption minimum with respect to the applied power density; and 3) we test the strategy of selecting optimal test conditions for determining model parameters T_{act} and z_c.

2. Review of ADT CHEETEH-E Model [17]

The ADT CHEETEH-E model was proposed in [17] for predicting heat-induced withdrawal reflex of a subject exposed to an electromagnetic beam. The computational framework starts at the radiation antenna which sends the millimeter

wave toward the skin surface of a subject, located at a certain distance away. Let N be the number of radiators in the antenna and $\wp_i$ be the power output of the i-th radiator. The power output of the antenna is described by the vector $\{\wp_i, i = 0, 1, \cdots, (N-1)\}$. We review the formulation components used in [17] for modeling sub-steps in the process from the electromagnetic power output of the antenna eventually to the subject's behavioral response.

1) Electric field near the skin of the subject

$$\underbrace{E(r)}_{\text{Electric field on skin at } r} = \sum_{i=0}^{N-1} \beta_i \sqrt{2\eta_0 \wp_i} \frac{1}{4\pi R_i} e^{\left(-\frac{\alpha}{2}R_i - jkR_i\right)} f\left(\hat{R}_i\right)$$

where:

- r is the position vector of a point on the skin surface of the subject;
- r_i is the position vector of the i-th radiator of the antenna;
- $R_i = |r - r_i|$ and $\hat{R}_i = \dfrac{r - r_i}{|r - r_i|}$ are respectively the magnitude and the unit direction of vector $(r - r_i)$;
- α is the atmospheric attenuation coefficient;
- $k = 2\pi/\lambda$ is the wave number of the electromagnetic wave; λ is the wave length; and $j = \sqrt{-1}$.

2) Power incident per area on the skin

$$\underbrace{P_{\text{incident}}(r)}_{\text{Power incident per area on skin at } r} = \frac{|E(r)|^2}{2\eta_0}$$

3) Power deposited per area on the skin

$$\underbrace{P_{\text{dep}}(r)}_{\text{Power deposited per area on skin at } r} = (1 - \gamma) P_{\text{incident}}(r)$$

4) Power absorbed per volume into the skin

$$\underbrace{q(r, y)}_{\text{Power absorbed per volume into skin at depth } y} = P_{\text{dep}}(r) \mu e^{-\mu y}$$

where y is the coordinate of depth from the skin surface and $1/\mu$ is the characteristic depth that the millimeter wave penetrates into the skin. In the formulation here r is a vector in $\mathbb{R}^3$, restricted to the 2-D skin surface, describing the 2-D coordinates on the skin surface. In a local 3-D coordinate system with the depth direction selected as an axis, r is effectively a vector in $\mathbb{R}^2$, and mathematically (r, y) represents the 3-D coordinates in the skin.

5) Temperature as a function of spatial coordinates and time

The temperature distribution is governed by the heat conduction along the depth direction with a source term of electromagnetic heating.

$$\begin{cases} \rho C_p \dfrac{\partial T(r, y, t)}{\partial t} = \dfrac{\partial}{\partial y}\left(K \dfrac{\partial T(r, y, t)}{\partial y} \right) + q(r, y) \\ \left. \dfrac{\partial T(r, y, t)}{\partial y} \right|_{y=0} = 0, \quad T(r, y, 0) = T_0(y) \end{cases}$$

where

- ρ is the mass density of the subject's skin;
- C_p is the specific heat capacity of the skin and;
- K is the thermal conductivity of the skin.

In the initial boundary value problem above, an insulated boundary condition is imposed at the skin surface ($y = 0$).

6) Number of heat-sensitive nociceptors activated in a local voxel

Each small voxel either has all its heat-sensitive nociceptors activated or has none of them activated depending on the average temperature.

$$\underbrace{x_j(t)}_{\text{Number of nociceptors activated in voxel } j} = \begin{cases} V_j \rho_{\text{noc}}, & \text{if } \overline{T_j}(t) \geq T_{\text{act}} \\ 0, & \text{if } \overline{T_j}(t) < T_{\text{act}} \end{cases}$$

where

- voxel j is a volume element in the computational discretization;
- V_j is the volume of voxel j;
- ρ_{noc} is the density of heat-sensitive nociceptors in the subject's skin;
- $\overline{T_j}(t)$ is the average temperature of voxel j at time t and;
- T_{act} is the activation temperature of heat-sensitive nociceptors.

7) Total number of heat-sensitive nociceptors activated at time t

$$\underbrace{x(t)}_{\text{Total number of nociceptors activated}} = \sum_{j=0}^{M-1} x_j(t)$$

where M is the number of voxels in the computational discretization.

8) Perceived pain level

$$\underbrace{h_{\text{Dol}}(t)}_{\text{Perceived pain level in Dol scale at time } t} = \frac{a}{1 + \exp\left(\frac{-(\ln x(t) - b)}{c}\right)}$$

9) Motivation-modulated perceived pain level

$$\underbrace{\hat{h}_{\text{Dol}}(t)}_{\text{Motivation modulated perceived pain level in Dol scale at time } t} = h_{\text{Dol}}(t) - \frac{m}{m_0}$$

10) Subject's behavioral response

$$\underbrace{g(t)}_{\substack{\text{Subject's behavioral} \\ \text{response at time } t}} = \begin{cases} 0 \ (\text{no movement}), & \text{if } \hat{h}_{\text{Dol}}(t) < Y_{\text{Low}} \\ 1 \ (\text{flinch but remain in beam}), & \text{if } Y_{\text{Low}} \leq \hat{h}_{\text{Dol}}(t) < Y_{\text{High}} \\ 2 \ (\text{move out of beam}), & \text{if } \hat{h}_{\text{Dol}}(t) \geq Y_{\text{High}} \end{cases}$$

3. A Concise Model for the Withdrawal Reflex

This section focuses on the occurrence of withdrawal reflex, observed as the subject moving out of beam in tests. At a given time t, we consider the event that the spatial temperature profile results in withdrawal reflex. In terms of the subject's behavioral response, this event is simply described by $\text{Event}\{g(t) = 2\}$. To formulate a concise model, we follow the model components proposed in

[17] as guidelines. We adopt the same assumption that the perceived pain level at time *t* is solely determined by the number of activated nociceptors at time *t*, which in turn is solely determined by the spatial temperature profile at time *t*. In other words, given the temperature profile at time *t*, the past history of the temperature profile does not affect the perceived pain level at time *t*. Our strategy is to use only the principles of these model components, not the specific function forms. The goal is to construct a formulation i) that is broadly applicable without assuming a particular function form for any internal sub-step and ii) that is concise with only a few model parameters. Specifically, we require the model to have 3 design features: [leftmargin = 1.5 cm].

- it maps a given spatial temperature profile to the corresponding binary outcome with regard to the occurrence of withdrawal reflex;
- it is independent of the function forms adopted in [17] and;
- it has only two parameters.

Building upon the model components of [17], we proceed with the analysis steps below.

- Based on the relation between $g(t)$ and $\hat{h}_{\mathrm{Dol}}(t)$ (the motivation-modulated perceived pain level) described in model component 10 above, we write.

$$\mathrm{Event}\left\{g(t)=2\right\} = \mathrm{Event}\left\{\hat{h}_{\mathrm{Dol}}(t) \ge Y_{\mathrm{High}}\right\}$$

- $\hat{h}_{\mathrm{Dol}}(t)$ is a monotonically increasing function of $h_{\mathrm{Dol}}(t)$ (the perceived pain level). In model component 9 above, this function is set to: $\hat{h}_{\mathrm{Dol}}(t) = h_{\mathrm{Dol}}(t) - m/m_0$. Here we write generally $\hat{h}_{\mathrm{Dol}}(t) = F_1\left(h_{\mathrm{Dol}}(t)\right)$ and require only that $F_1(\cdot)$ be an increasing function. Applying $F_1^{-1}(\cdot)$ to $\hat{h}_{\mathrm{Dol}}(t) \ge Y_{\mathrm{High}}$, we write:

$$\mathrm{Event}\left\{g(t)=2\right\} = \mathrm{Event}\left\{h_{\mathrm{Dol}}(t) \ge F_1^{-1}\left(Y_{\mathrm{High}}\right)\right\}$$

- $h_{\mathrm{Dol}}(t)$ increases monotonically with $x(t)$ (the total number of nociceptors activated). In model component 8 above, $h_{\mathrm{Dol}}(t)$ is set to:

$$h_{\mathrm{Dol}}(t) = \frac{a}{1 + \exp\left(\dfrac{-\left(\ln\left(x(t)\right) - b\right)}{c}\right)}.$$ Again, we write generally

$h_{\mathrm{Dol}}(t) = F_2\left(x(t)\right)$ and require only that $F_2(\cdot)$ be an increasing function. Applying $F_2^{-1}(\cdot)$ to $h_{\mathrm{Dol}}(t) \ge F_1^{-1}\left(Y_{\mathrm{High}}\right)$, we write:

$$\mathrm{Event}\left\{g(t)=2\right\} = \mathrm{Event}\left\{x(t) \ge F_2^{-1}\left(F_1^{-1}\left(Y_{\mathrm{High}}\right)\right)\right\}$$

- At a given time *t*, $x(t)$ is determined from the spatial temperature profile $T(\boldsymbol{r}, y, t)$:

$$x(t) = \rho_{\mathrm{noc}} \underbrace{\int I_{(T \ge T_{\mathrm{act}})}(\boldsymbol{r}, y, t)\,\mathrm{d}\boldsymbol{r}\,\mathrm{d}y}_{\text{Activated volume}}$$

where the indicator function $I_{(T \ge T_{\mathrm{act}})}$ is defined as:

$$I_{(T \geq T_{act})}(\boldsymbol{r}, y, t) \equiv \begin{cases} 1, & \text{if } T(\boldsymbol{r}, y, t) \geq T_{act} \\ 0, & \text{if } T(\boldsymbol{r}, y, t) < T_{act} \end{cases}$$

Using this expression of $x(t)$, we write the event in terms of $T(\boldsymbol{r}, y, t)$:

$$\text{Event}\{g(t) = 2\} = \text{Event}\left\{ \int I_{(T \geq T_{act})} \mathrm{d}\boldsymbol{r}\mathrm{d}y \geq \frac{1}{\rho_{noc}} F_2^{-1}\left(F_1^{-1}\left(Y_{High}\right) \right) \right\} \quad (1)$$

Result (1) leads to a deterministic dose-response relation for withdrawal reflex. Given spatial temperature profile $T(\boldsymbol{r}, y)$, we select the activated volume as the single metric predictor variable (the dose quantity) for predicting withdrawal reflex.

$$\underbrace{z \equiv z(\{T\}, T_{act})}_{\text{Dose}} \equiv \underbrace{\int I_{(T \geq T_{act})} \mathrm{d}\boldsymbol{r}\mathrm{d}y}_{\text{Activated volume}} \quad (2)$$

Here we use $\{T\}$ as a concise notation for spatial temperature profile $T(\boldsymbol{r}, y)$. Equation (1) tells us that the critical threshold on dose z for withdrawal reflex is

$$z_c \equiv \frac{1}{\rho_{noc}} F_2^{-1}\left(F_1^{-1}\left(Y_{High}\right) \right) \quad (3)$$

The deterministic dose-response model is

$$\text{Outcome}(z) = \begin{cases} 1 \, (\text{withdrawal reflex}), & \text{if } z \geq z_c \\ 0 \, (\text{no withdrawal reflex}), & \text{if } z < z_c \end{cases} \quad (4)$$

Model (4) is completely specified by 2 parameters: T_{act} and z_c.

- Activation temperature T_{act} is used in calculating dose z in (2).
- Threshold z_c is used in determining the binary outcome corresponding to dose z.

Note that threshold z_c varies with many internal parameters of ADT CHEE-TEH-E [17]:

- Y_{High} in the subject behavioral response function $g(t)$;
- m and m_0 in the motivation modulated perceived pain level $\hat{h}_{Dol}(t)$;
- a, b and c in the perceived pain level $h_{Dol}(t)$ and;
- ρ_{noc} in the total number of nociceptors activated $x(t)$.

In addition, threshold z_c depends on function forms of $F_1(\cdot)$ and $F_2(\cdot)$. The advantage of model (4) is that the effect of all these model parameters and function forms is captured in a single parameter z_c. Once the values of z_c and T_{act} are known, dose-response model (4) is completely specified.

4. Inferring Model Parameters from Spatial Temperature Profiles

We study the methodology of determining the two parameters (z_c and T_{act}) in model (4) from test data. We consider the hypothetical situation where the temperature of the skin as a function of the 3-D coordinates and the time is measurable in experiments.

The dose-response model described in (4) is based on the assumption that the occurrence of withdrawal reflex at time t_{ref} is solely attributed to the spatial temperature profile at t_{ref}. As a result, in the inference method, only $T(\boldsymbol{r}, y, t_{\text{ref}})$ is relevant for determining T_{act} and z_c. In experimental setup, two quantities are tunable: the power density deposited on the skin surface P_{dep} and the beam spot area A. When the applied power density is uniform inside a geometric area and zero outside, the beam spot is naturally defined as that area. When the applied power density is a function of the 2-D coordinates on the skin surface: $P_{\text{dep}} = P_{\text{dep}}(\boldsymbol{r})$, the scalar beam spot area A refers to a characteristic area of the beam cross-section. For a Gaussian beam with radius w, the beam spot may refer to the circle of radius w around the beam center, which is the region of $P_{\text{dep}}(\boldsymbol{r}) \geq \frac{1}{e^2} P_{\text{dep}}(0)$ or equivalently the region of $E(\boldsymbol{r}) \geq \frac{1}{e} E(0)$. Alternatively, the beam spot area may refer to the peak effective area, which is defined as $A \equiv \int_{\mathbb{R}^2} P_{\text{dep}}(\boldsymbol{r}) \mathrm{d}\boldsymbol{r} / P_{\text{dep}}(0)$.

In test data, information on the unknown parameters T_{act} and z_c is contained in the reflex time t_{ref} and in the spatial temperature profile at reflex $T(\boldsymbol{r}, y, t_{\text{ref}})$. For a given $T(\boldsymbol{r}, y, t_{\text{ref}})$, we can set the activation temperature T_{act} to any reasonable value within the range of $T(\boldsymbol{r}, y, t_{\text{ref}})$. Then, for each value of T_{act}, the threshold $z_c(T_{\text{act}})$ is the activated volume calculated according to T_{act}.

$$z_c(T_{\text{act}}) \equiv \text{volume of } \left\{ (\boldsymbol{r}, y) \middle| T(\boldsymbol{r}, y, t_{\text{ref}}) \geq T_{\text{act}} \right\} \tag{5}$$

Function $z_c(T_{\text{act}})$ defined in (5) is based on the temperature profile $T(\boldsymbol{r}, y, t_{\text{ref}})$. Given $T(\boldsymbol{r}, y, t_{\text{ref}})$, the pair $(T_{\text{act}}, z_c(T_{\text{act}}))$ explains the observed reflex time t_{ref} for any value of T_{act}. In other words, one temperature profile $T(\boldsymbol{r}, y, t_{\text{ref}})$ does not provide enough information for determining both T_{act} and z_c simultaneously. At a given test condition, the measurements provide only one constraint function $z_c(T_{\text{act}})$ on the two unknown parameters. When the test condition $(\{P_{\text{dep}}(\boldsymbol{r})\}, A)$ is varied in experiments, the reflex time t_{ref} and the temperature profile at reflex $T(\boldsymbol{r}, y, t_{\text{ref}})$ will change, and accordingly, the constraint function $z_c(T_{\text{act}})$ may be different. The influence of test condition on the constraint function $z_c(T_{\text{act}})$ offers hope of constructing substantially distinct equations for (T_{act}, z_c) from data measured at different test conditions. Once we obtain two different constraint equations for (T_{act}, z_c), the two unknown parameters are solved simultaneously from a 2×2 system.

$$\begin{cases} z_c - z_c(T_{\text{act}}) \big|_{(\text{test condition 1})} = 0 \\ z_c - z_c(T_{\text{act}}) \big|_{(\text{test condition 2})} = 0 \end{cases} \tag{6}$$

Let us summarize and clarify what information regarding model parameters (z_c, T_{act}) we can extract from measured temperature profiles and how we extract it.

- At a given test condition $(\{P_{\text{dep}}(\boldsymbol{r})\}, A)$, the two unknown parameters T_{act}

and z_c are constrained by only one function: $z_c(T_{act})$.

- As described in (5), constraint function $z_c(T_{act})$ is completely determined by the measured spatial temperature profile $T(\boldsymbol{r}, y, t_{ref})$. Function $z_c(T_{act})$ is parameter-free.

- In the subsequent sections, we will analyze the behaviors of $z_c(T_{act})$ in certain idealized cases. It is important to point out that the construction of $z_c(T_{act})$, given in (5), is not dependent on the assumptions of these idealized cases. The assumptions are for the purpose of facilitating the exact solution of temperature evolution.

- If test data from different test conditions provide two distinct constraint equations, then parameters (T_{act}, z_c) can be determined from the 2×2 system (6).

In the next section, we will explore theoretically what test conditions are likely to provide substantially distinct constraint equations for (T_{act}, z_c). To make it possible to solve the problem analytically, we will introduce assumptions and consider idealized cases in the analysis. The results of the mathematical study on these idealized cases are only intended as guidelines for selecting test conditions that will (in the idealized cases) provide substantially distinct constraint equations for (T_{act}, z_c). Once the tests are carried out and measurements are collected, the construction of constraint equations $z_c(T_{act})$ is based on the real test data using formula (5), which does not depend on any assumption used in the idealized cases. The process of determining (T_{act}, z_c) is solely based on measured temperature profiles at several test conditions. It does not require any symmetry of temperature or any particular parameter values for the heat absorption/conduction in the skin.

5. Theoretical Behaviors of the System in the Case of No Heat Conduction

In this section, we study the case of no heat conduction. We examine the behaviors of the temperature distribution, the time until reflex, the latency in withdrawal reflex, and the constraint function on model parameters based on the spatial temperature profile at reflex. To facilitate the analysis in a simple theoretical setting, we first introduce idealized cases.

5.1. Idealized Case U and Case A

Idealized case U is characterized by the two assumptions below:

1) At any given time, the temperature is uniform over the beam cross-section A (*i.e.*, independent of $\boldsymbol{r}$) and is a decreasing function of depth y.

2) Outside the beam cross-section, the temperature is always below the nociceptor activation temperature (for example, at the normal body temperature).

One particular situation of case U is when the initial temperature of skin is a constant below the activation temperature and the applied power density is uniform over the beam cross-section A and zero outside. Mathematically, idealized

case U is characterized by

$$
\text{Case U} \equiv \begin{cases} T(\boldsymbol{r}, y, t) = T(y, t), \text{ decreasing with } y, \text{ for } \boldsymbol{r} \in A \\ T(\boldsymbol{r}, y, t) < T_{\text{act}}, \text{ for } \boldsymbol{r} \notin A \end{cases} \tag{7}
$$

In case U, it is mathematically more convenient to view the constraint function in the form of $T_{\text{act}}(z_c)$ with z_c as the independent variable. Recall that the dose z is defined as the volume of the activated region, which in case U is a cylinder with base area A. Dose z has the expression: $\text{volume} = \text{base} \times \text{depth}$. Given the threshold z_c on activated volume and the beam spot area A, the corresponding activated depth is $y_{\text{act}} = z_c / A$. The activation temperature T_{act}, and $(y_{\text{act}}, t_{\text{ref}})$ are related in the temperature distribution $T(y, t)$

$$
\text{Case U}: T_{\text{act}} = T\left(\frac{z_c}{A}, t_{\text{ref}}\right) \equiv T_{\text{act}}(z_c) \tag{8}
$$

Equation (8) serves various purposes depending on which are known/unknown. On one hand, given the reflex time t_{ref} and the spatial temperature profile at reflex $T(y, t_{\text{ref}})$, (8) is a constraint equation for model parameters (T_{act}, z_c). On the other hand, given model parameters (T_{act}, z_c), (8) is an equation for the reflex time t_{ref}. We will use this equation to solve for t_{ref} in case A and case B below, which are special situations of case U. Notice that constraint function $T_{\text{act}}(z_c)$ given by (8) in case U is simply the temperature profile at reflex, scaled in the depth direction by a factor of $1/A$. Based on the mathematical form of (8), intuitively we can change how fast $T_{\text{act}}(z_c)$ varies with z_c by reducing/increasing beam spot area A in experiments.

It should be mentioned that case U does not exclude heat conduction in the depth direction. We now add the assumption of no-heat-conduction and introduce case A.

$$
\text{Case A} \equiv \begin{cases} \text{uniform power density over beam spot}: \\ \quad P_{\text{dep}}(\boldsymbol{r}) = P_{\text{dep}} \text{ for } \boldsymbol{r} \in A \text{ and } P_{\text{dep}}(\boldsymbol{r}) = 0 \text{ for } \boldsymbol{r} \notin A \\ \text{no heat conduction} \\ \text{uniform initial temperature}: T(y, 0) = T_0 < T_{\text{act}} \end{cases} \tag{9}
$$

Case A satisfies the conditions of case U, and is a special situation of case U.

5.2. Selecting Test Conditions for Determining (T_{act}, z_c)

Case A is solved analytically in **Appendix A**. The temperature distribution and the reflex time are given by (see Equations (65) and (66) of **Appendix A**).

$$
\text{Results of case A}: \begin{cases} T(\boldsymbol{r}, y, t) = T_0 + t \dfrac{P_{\text{dep}} \mu}{\rho C_p} e^{-\mu y} & \text{for } \boldsymbol{r} \in A \\ t_{\text{ref}} = \dfrac{T_{\text{act}} - T_0}{P_{\text{dep}}} \cdot \dfrac{\rho C_p}{\mu} e^{\mu z_c / A} \end{cases} \tag{10}
$$

It follows from (8) that the constraint function $T_{\text{act}}(z_c)$ has the expression

$$T_{\text{act}}(z_c) = T_0 + \frac{t_{\text{ref}} P_{\text{dep}} \mu}{\rho C_p} e^{-\mu z_c / A} \tag{11}$$

Let $\left(T_{\text{act}}^*, z_c^*\right)$ denote the true value of $\left(T_{\text{act}}, z_c\right)$. With this specific notation for the true values, we can use z_c to represent the independent variable and T_{act} the dependent variable in constraint function $T_{\text{act}}(z_c)$ without confusion. We like to get rid of $\frac{t_{\text{ref}} P_{\text{dep}} \mu}{\rho C_p}$ in (11) by using $\left(T_{\text{act}}^*, z_c^*\right)$. In the inference method, we view (11) as a constraint function on $\left(z_c, T_{\text{act}}\right)$ while t_{ref} is known (from data). Alternatively (11) may be viewed as the governing equation for t_{ref} when z_c^* and T_{act}^* are given. We use (11) to express t_{ref} in terms of $\left(T_{\text{act}}^*, z_c^*\right)$ and then substitute the expression back into (11) to write constraint function $T_{\text{act}}(z_c)$ as

$$T_{\text{act}}(z_c) = T_0 + \left(T_{\text{act}}^* - T_0\right) e^{\mu z_c^* / A} \cdot e^{-\mu z_c / A}$$

We cast the constraint function into the form of $\left(T_{\text{act}} - T_{\text{act}}^*\right)$ vs. $\left(z_c - z_c^*\right)$

$$T_{\text{act}}(z_c) - T_{\text{act}}^* = \left(T_{\text{act}}^* - T_0\right) \cdot \left(e^{-\mu\left(z_c - z_c^*\right)/A} - 1\right) \tag{12}$$

Constraint function (12) is specified by two parameters: $\left(T_{\text{act}}^* - T_0\right)$ and A/μ. Note that (12) is the constraint function for case A (the case of no heat conduction) and it is independent of the power density P_{dep}, which specifies how fast the electromagnetic beam heats up the skin. When the effect of heat conduction along the depth direction is included, P_{dep} will affect the steepness of spatial temperature profile at reflex. A smaller power density P_{dep} heats up the skin slower and the heat conduction has more time before reflex to smooth out the temperature profile.

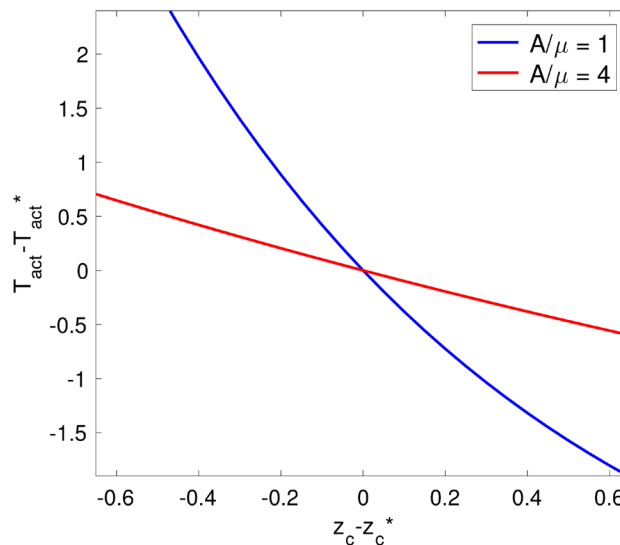**Figure 1** compares constraint functions constructed from simulated test data

Figure 1. Constraint functions on $\left(T_{\text{act}}, z_c\right)$ based on simulated data in case A. The intersection of two distinct constraint functions determines the true values $\left(T_{\text{act}}^*, z_c^*\right)$.

in case A, with two different beam spot areas: $A/\mu = 1$ and $A/\mu = 4$. The well-defined intersection of the two curves gives us the true value T_{act}^* and z_c^*. In simulations, we used $\left(T_{\text{act}}^* - T_0\right) = 4$. The choice of $\left(T_{\text{act}}^* - T_0\right)$ does not actually alter the essential shape of constraint functions. If we divide (12) by $\left(T_{\text{act}}^* - T_0\right)$ and use the scaled temperature as the dependent variable, then (12) is completely specified by A/μ, independent of $\left(T_{\text{act}}^* - T_0\right)$.

In summary, in case A, to determine model parameters T_{act} and z_c, we need to carry out tests with different beam spot areas: one with a moderate value of A/μ to make the constraint function T_{act} vs. z_c slant, the other with a relatively large value of A/μ to make T_{act} vs. z_c flat. Notice that the meanings of phrases "moderate value of A/μ" and "relatively large value of A/μ" are not precise since quantity A/μ is not dimensionless. This issue will be addressed when we discuss non-dimensionalization.

5.3. Time until Withdrawal Reflex vs. Beam Spot Area

We study how the reflex time t_{ref} varies with the beam spot area A while the power density P_{dep} is maintained at a constant level. In case A (the case of no heat conduction), the analytical expression of t_{ref} is given in (10). In expression (10), when the beam spot area A is fixed, the reflex time t_{ref} is inversely proportional to the applied power density P_{dep}. When P_{dep} is fixed, as beam spot area A increases, t_{ref} decreases. But t_{ref} is not inversely proportional to A. Eventually t_{ref} reaches a constant level above zero for large A. This can be seen in the Taylor expansion of (10) as $(1/A) \to 0$.

Case A: no heat conduction

$$t_{\text{ref}} = \frac{T_{\text{act}} - T_0}{P_{\text{dep}}} \cdot \frac{\rho C_p}{\mu}\left(1 + \frac{\mu z_c}{A} + O\left(A^{-2}\right)\right) \tag{13}$$

In all realistic situations, heat conduction is always present. Case A (the case of no heat conduction) corresponds to the situation where the effect of heat conduction is relatively small in comparison with others. In the non-dimensional analysis of the next section, we will see that the effect of heat conduction is negligible only in a region away from the skin surface and only over a short time. Even during a short time, near skin surface, the heat conduction may still be significant or even dominant in the temperature evolution. Expression (10) for t_{ref} is derived based on the no-conduction approximation of the temperature at depth z_c/A. For large A, depth z_c/A is close to the skin surface. As a result, expression (10) for t_{ref} eventually becomes invalid for large A. Expanding t_{ref} vs. A with the effect of heat conduction will be carried out after the non-dimensionalization analysis. We will see that with the effect of heat conduction, the $(1/A)$ term in expansion (13) is invalid.

5.4. Latency in Withdrawal Reflex

We hypothesize that when the number of nociceptors activated reaches a threshold, the stimulus sent to the Central Nervous System (CNS) is strong enough

to initiate the withdrawal reflex. However, it takes time for the signal to travel to the CNS, for the CNS to send a signal to muscles, and for muscles to act upon the signal to carry out the withdrawal reflex before the actual withdrawal reflex action (*i.e.*, the subject moving out of the beam) is observed in tests. To facilitate the discussion of biological latency in the observed withdrawal reflex, we first introduce proper mathematical notations for these time instances. Let

- t_{ref} = time until the activated volume (dose *z*) reaches threshold z_c; t_{ref} is the time until a stimulus strong enough for initiating withdrawal reflex is generated; we regard t_{ref} as the true underlying reflex time in the sense that even if the beam power is turned off at that point, withdrawal reflex will still occur;

- t_{obs} = time until observed withdrawal reflex; t_{obs} is the observed reflex time;

- $t_{\text{del}} = t_{\text{obs}} - t_{\text{ref}}$ = latency (time delay) in the observed withdrawal reflex.

We assume that the time delay t_{del} is an intrinsic property of the test subject, not affected by parameters of the electromagnetic beam, such as power density (P_{dep}) or beam spot area (*A*). In case A (the case of no heat conduction), the true underlying reflex time t_{ref} is given by (10). The observed reflex time t_{obs} has the expression:

$$t_{\text{obs}} = \frac{T_{\text{act}} - T_0}{P_{\text{dep}}} \cdot \frac{\rho C_p}{\mu} e^{\mu z_c / A} + t_{\text{del}} \tag{14}$$

The plot of t_{obs} vs $1/P_{\text{dep}}$ is a straight line. The vertical intercept of the plot gives us t_{del}, which can be estimated from measured values of t_{obs} at $P_{\text{dep}} = p_0$ and $P_{\text{dep}} = 2p_0$.

Case A: no heat conduction

$$t_{\text{del}}^{(\text{est})} = 2t_{\text{obs}}(2p_0) - t_{\text{obs}}(p_0). \tag{15}$$

6. Non-Dimensionalization and Solution of Heat Conduction in the Depth Direction

We study the effect of heat conduction along the depth direction of the skin (the *y*-direction of the coordinate system). We first introduce case B which has all assumptions of case A except that it includes the effect of heat conduction in the depth direction with uniform thermal conductivity: $K(y) \equiv K$.

$$\text{Case B} \equiv \left\{ \begin{array}{l} \text{uniform power density over beam spot :} \\ \quad P_{\text{dep}}(\boldsymbol{r}) = P_{\text{dep}} \text{ for } \boldsymbol{r} \in A \text{ and } P_{\text{dep}}(\boldsymbol{r}) = 0 \text{ for } \boldsymbol{r} \notin A \\ \text{heat conduction in } y \text{ with uniform conductivity} \\ \text{uniform initial temperature : } T(y,0) = T_0 < T_{\text{act}} \end{array} \right\} \tag{16}$$

In case B, the temperature distribution is governed by

$$\left\{ \begin{array}{l} \rho C_p \dfrac{\partial T(\boldsymbol{r}, y, t)}{\partial t} = K \dfrac{\partial^2 T(\boldsymbol{r}, y, t)}{\partial y^2} + P_{\text{dep}} \mu e^{-\mu y} \quad \text{for } \boldsymbol{r} \in A \\ \left. \dfrac{\partial T(\boldsymbol{r}, y, t)}{\partial y} \right|_{y=0} = 0, \quad T(\boldsymbol{r}, y, 0) = T_0 \end{array} \right. \tag{17}$$

6.1. Non-Dimensionalization

We introduce a temperature scale ΔT, the characteristic difference between the initial temperature T_0 and the nociceptor activation temperature T_{act}. Note that ΔT serves only as the temperature scale for non-dimensionalization. ΔT does not need to be the exact difference between T_0 and T_{act}. We look at the physical dimensions of various quantities:

$$[\mu] = (\text{length})^{-1}$$

$$[K] = (\text{energy})(\text{temperature})^{-1}(\text{length})^{-1}(\text{time})^{-1}$$

$$[\rho C_p] = (\text{energy})(\text{temperature})^{-1}(\text{length})^{-3}$$

$$\left[\frac{K}{\rho C_p}\right] = (\text{length})^2(\text{time})^{-1}$$

$$\left[\frac{K\mu^2}{\rho C_p}\right] = (\text{time})^{-1}$$

$$\left[P_{\text{dep}}\right] = (\text{energy})(\text{length})^{-2}(\text{time})^{-1}$$

$$[\Delta T] = (\text{temperature})$$

$$\left[\frac{1}{K\mu\Delta T}\right] = (\text{energy})^{-1}(\text{length})^2(\text{time}) = \frac{1}{\left[P_{\text{dep}}\right]}$$

We introduce length scale and time scale

$$y_{\text{s}} \equiv \frac{1}{\mu}, \quad t_{\text{s}} \equiv \frac{\rho C_p}{K\mu^2}$$

Here y_{s} is the depth at which the beam decays by a factor of e^{-1}, and t_{s} is the time at which a δ function spreads to a Gaussian distribution of standard deviation y_{s}. We use these characteristic scales to carry out non-dimensionalization.

Non-dimensional depth and time:

$$y_{\text{nd}} \equiv \frac{y}{y_{\text{s}}} = \mu y, \quad t_{\text{nd}} \equiv \frac{t}{t_{\text{s}}} = t\frac{K\mu^2}{\rho C_p}$$

Non-dimensional temperature as a function of $(y_{\text{nd}}, t_{\text{nd}})$:

$$T_{\text{nd}}(y_{\text{nd}}, t_{\text{nd}}) \equiv \frac{T(y,t) - T_0}{\Delta T}$$

Non-dimensional reflex time:

$$t_{\text{ref,nd}} \equiv \frac{t_{\text{ref}}}{t_{\text{s}}} = t_{\text{ref}}\frac{K\mu^2}{\rho C_p}$$

Non-dimensional power density deposited on skin surface:

$$P_{\text{dep,nd}} \equiv P_{\text{dep}}\frac{1}{K\mu\Delta T}$$

Non-dimensional beam spot area:

$$A_{\text{nd}} \equiv A\frac{y_{\text{s}}}{z_c} = A\frac{1}{\mu z_c}$$

Non-dimensional activation temperature:

$$T_{\text{act,nd}} \equiv \frac{T_{\text{act}} - T_0}{\Delta T}$$

The governing equation for $T_{\text{nd}}\left(y_{\text{nd}}, t_{\text{nd}}\right)$ follows from Equation (17).

$$\begin{cases} \dfrac{\partial T_{\text{nd}}}{\partial t_{\text{nd}}} = \dfrac{\partial^2 T_{\text{nd}}}{\partial y_{\text{nd}}^2} + P_{\text{dep,nd}} \exp\left(-y_{\text{nd}}\right) \\ \left.\dfrac{\partial T_{\text{nd}}}{\partial y_{\text{nd}}}\right|_{y_{\text{nd}}=0} = 0, \quad T\left(y_{\text{nd}}, 0\right) = 0 \end{cases} \tag{18}$$

The non-dimensional temperature distribution offers two mathematical advantages.

- For $T_{\text{nd}}\left(y_{\text{nd}}, t_{\text{nd}}\right)$, both the initial and the boundary conditions are homogeneous.

- $T_{\text{nd}}\left(y_{\text{nd}}, t_{\text{nd}}\right)$ is proportional to $P_{\text{dep,nd}}$. Function $T_{\text{nd}}\left(y_{\text{nd}}, t_{\text{nd}}\right)/P_{\text{dep,nd}}$ is parameter-free. The effects of all other parameters are contained in the non-dimensional variables.

We define the normalized non-dimensional temperature

$$H\left(y, t\right) \equiv \frac{1}{P_{\text{dep,nd}}} T_{\text{nd}}\left(y, t\right) \tag{19}$$

Here we have denoted $\left(y_{\text{nd}}, t_{\text{nd}}\right)$ concisely as $\left(y, t\right)$. Function $H\left(y, t\right)$ is governed by

$$\begin{cases} \dfrac{\partial H}{\partial t} = \dfrac{\partial^2 H}{\partial y^2} + \mathrm{e}^{-y} \\ \left.\dfrac{\partial H}{\partial y}\right|_{y=0} = 0, \quad H\left(y, 0\right) = 0 \end{cases} \tag{20}$$

Notice that the normalized Equation (20) is parameter-free.

6.2. Analytical Solution

To solve problem (20), we view the forcing term as the time integral of impulse forcing. Let $G\left(y, t\right)$ denote the solution of a unit impulse forcing at $t = 0$, which is governed by

$$\begin{cases} \dfrac{\partial G}{\partial t} = \dfrac{\partial^2 G}{\partial y^2} \\ \left.\dfrac{\partial G}{\partial y}\right|_{y=0} = 0, \quad G\left(y, 0\right) = \mathrm{e}^{-y} \end{cases} \tag{21}$$

In **Appendix B**, we derive that $G\left(y, t\right)$ has the expression

$$G\left(y, t\right) = \frac{1}{2}\text{erfc}\left(\frac{2t - y}{\sqrt{4t}}\right)\mathrm{e}^{t-y} + \frac{1}{2}\text{erfc}\left(\frac{2t + y}{\sqrt{4t}}\right)\mathrm{e}^{t+y}$$

where $\mathrm{erfc}(\cdot)$ is the complementary error function defined as

$$\mathrm{erfc}(x) \equiv \frac{2}{\sqrt{\pi}} \int_x^\infty \exp(-s^2)\,\mathrm{d}s$$

We integrate $G(y, t-s)$ with respect to s to superpose the effect of forcing in $[0, t]$. The solution of problem (20) is given by

$$H(y,t) = \int_0^t G(y, t-s)\,\mathrm{d}s = \int_0^t G(y, s)\,\mathrm{d}s$$

Function $H(y,t)$ satisfies:

(i) At each fixed y, $H(y,t)$ is an increasing function of t.

(ii) At each fixed t, $H(y,t)$ is a decreasing function of y.

(iii) At a fixed y, for small t, $H(y,t)$ increases with t more than linearly; for large t, the increase is slower than linear.

The third property of $H(y,t)$ illustrates the two opposite effects of heat conduction. In the absence of heat conduction, the heating term e^{-y} leads to a linearly increasing temperature $t\mathrm{e}^{-y}$. With heat conduction, at a fixed depth y, function $G(y,t)$ starts at $G(y,0) = \mathrm{e}^{-y}$ and increases over short time. As a result, $H(y,t)$ initially rises faster than $t\mathrm{e}^{-y}$. Over long time, however, heat conduction eventually pulls $G(y,t)$ back below e^{-y} and reduces it gradually to zero. Consequently, for large t, $H(y,t)$ grows much slower than $t\mathrm{e}^{-y}$ with growth rate decreasing toward zero. We will revisit property (iii) and derive the behaviors of $H(y,t)$ respectively for small t and for large t in the asymptotic analysis of the next section.

In summary, in case B (the case with heat conduction), $T_{\mathrm{nd}}(y_{\mathrm{nd}}, t_{\mathrm{nd}})$ has the expression

$$\text{Results of case B}:\begin{cases} T_{\mathrm{nd}}(y_{\mathrm{nd}}, t_{\mathrm{nd}}) = P_{\mathrm{dep,nd}} H(y_{\mathrm{nd}}, t_{\mathrm{nd}}) \\ H(y,t) = \int_0^t G(y,s)\,\mathrm{d}s \\ G(y,t) = \frac{1}{2}\mathrm{erfc}\left(\frac{2t-y}{\sqrt{4t}}\right)\mathrm{e}^{t-y} + \frac{1}{2}\mathrm{erfc}\left(\frac{2t+y}{\sqrt{4t}}\right)\mathrm{e}^{t+y} \end{cases} \tag{22}$$

The pre-scaling physical temperature distribution $T(y,t)$ is

$$T(y,t) - T_0 = \Delta T \cdot P_{\mathrm{dep,nd}} H\left(\frac{y}{y_s}, \frac{t}{t_s}\right) = P_{\mathrm{dep}} \frac{1}{K\mu} H\left(\mu y, t\frac{K\mu^2}{\rho C_p}\right) \tag{23}$$

Equation (23) expresses the physical temperature distribution $T(y,t)$ as a scaling and shifting of the normalized non-dimensional temperature $H(y,t)$, which is parameter-free.

6.3. Effect of Heat Conduction

We investigate the consequence of neglecting heat conduction (*i.e.*, completely turning off the heat conduction in Equation (20)). Specifically, we remove the $\frac{\partial^2 H}{\partial y^2}$ term and the insulated boundary condition in (20). The resulting equa-

tion is

$$\frac{\partial H_0}{\partial t} = \mathrm{e}^{-y}, \quad H_0(y,0) = 0 \tag{24}$$

which yields the no-conduction approximation of $H(y,t)$

$$H_0(y,t) = t\mathrm{e}^{-y} \tag{25}$$

It is important to clarify the precise difference between Equations (20) and (24). They do not correspond to different regimes of heat conductivity. Rather, they are both obtained in non-dimensionalization using exactly the same parameters. The only difference is that at the end, in Equation (24) we discard the terms involving heat conduction.

To assess the validity of neglecting heat conduction, we compare $H_0(y,t)$ with $H(y,t)$ in **Figure 2** at several time instances. Here y and t are the non-dimensional depth and time. When t is small and y is away from 0, $H_0(y,t)$, provides a good approximation to $H(y,t)$.

We examine the relative error in approximating $H(y,t)$ with $H_0(y,t)$.

$$\mathrm{Err}(y,t) \equiv \frac{H_0(y,t) - H(y,t)}{H(y,t)} \tag{26}$$

Figure 3 plots contour lines of relative error $\mathrm{Err}(y,t)$ in percentage. Again, here y and t are the non-dimensional depth and time. The results illustrate regions where the relative error is bounded by the specified values.

For the physical temperature distribution, the no-conduction approximation is

$$(T(y,t) - T_0) \approx P_{\mathrm{dep}} \frac{1}{K\mu} H_0\left(\mu y, t\frac{K\mu^2}{\rho C_p}\right) = t\frac{P_{\mathrm{dep}}\mu}{\rho C_p} \mathrm{e}^{-\mu y} \tag{27}$$
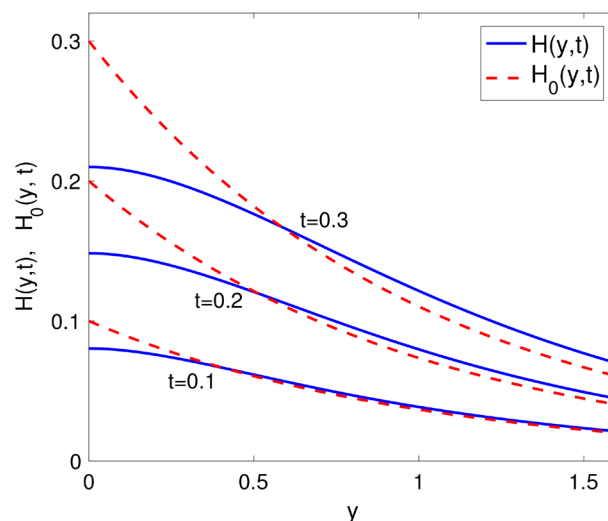

Figure 2. Comparison of $H(y,t)$ and $H_0(y,t)$, respectively, the normalized non-dimensional temperatures and its no-conduction approximation.
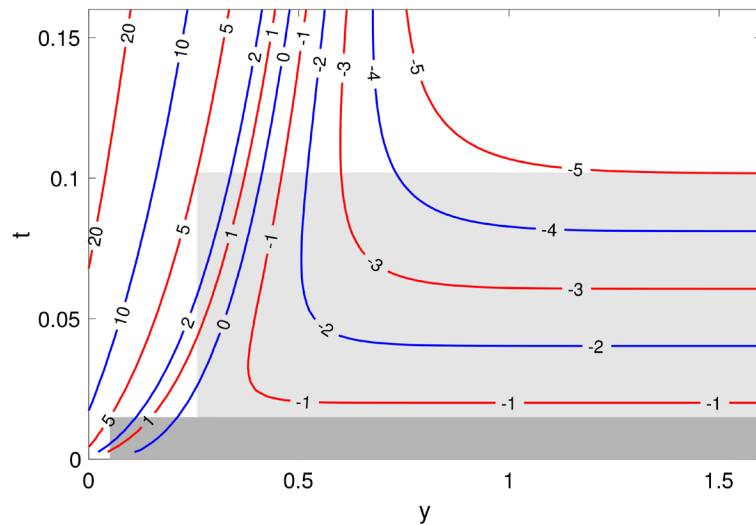
Figure 3. Contour lines of relative error $\text{Err}(y,t)$ defined in (26), in percentage.

Approximation (27) is valid when the non-dimensional time $t_{\text{nd}} \equiv t\dfrac{K\mu^2}{\rho C_p}$ is small and the non-dimensional depth $y_{\text{nd}} \equiv \mu y$ is away from 0. In the rectangular region of $t_{\text{nd}} \leq 0.102$ and $y_{\text{nd}} \geq 0.258$ (lightly shaded in **Figure 3**), the relative error in the no-conduction approximation of $\left(T(y,t)-T_0\right)$ is bounded by 5%. No-conduction approximation (27) is valid only at depth away from the skin surface. When depth y_{nd} is small (near skin surface), we need to restrict t_{nd} to a very small range in order to maintain a reasonably low relative error $\text{Err}(y,t)$. For example, at depth $y_{\text{nd}} = 0.05$, to make the relative error bounded by 5%, we have to restrict the non-dimensional time to the tiny interval of $t_{\text{nd}} \leq 0.015$ (darkly shaded rectangle in **Figure 3**).

7. Theoretical Behaviors of the System in the Case with Heat Conduction

In this section, we study the behaviors of case B (the case with heat conduction), based on its analytical solution. We examine the reflex time vs. beam spot area, the latency in withdrawal reflex, asymptotics of the normalized temperature for small *t* and for large *t*, the energy consumption at small and at large applied power density, the spatial temperature profile at reflex, and constraint functions constructed from spatial temperature profiles.

7.1. Reflex Time vs. Beam Spot Area

In subsection 5.3, we studied the asymptotic behavior of reflex time for large beam spot in case A (the case of no heat conduction). The asymptotic result of t_{ref} vs *A* in case A is given in (13). The derivation of (13) is based on the no-conduction approximation at depth z_c/A and time t_{ref}. As we discussed in subsection 6.3, the no-conduction approximation is valid only in the region away from the skin surface and only over short time. When we increase the

beam spot area A, the depth z_c/A converges to zero and the time t_{ref} decreases to a positive value above zero. For large A, the combination of depth z_c/A and time t_{ref} leads to a large relative error in the no-conduction approximation. Thus, when the beam spot is large, the no-conduction approximation is no longer valid. We now analyze the asymptotic behavior of t_{ref} for large A in the presence of heat conduction (case B).

In case U defined in (7), which includes case B, the governing equation for t_{ref} is given in (8). Using the exact solution (23) for case B, we write the equation in terms of the normalized temperature distribution $H(y,t)$:

$$T_0 + P_{\text{dep}} \frac{1}{K\mu} H\left(\frac{\mu z_c}{A}, t_{\text{ref}} \frac{K\mu^2}{\rho C_p} \right) = T_{\text{act}}$$

which leads to a non-dimensional equation for $t_{\text{ref,nd}}$

$$\frac{(T_{\text{act}} - T_0)K\mu}{P_{\text{dep}}} = H\left(\frac{1}{A_{\text{nd}}}, t_{\text{ref,nd}} \right) \tag{28}$$

where $A_{\text{nd}} = \dfrac{A}{\mu z_c}$ is the non-dimensional beam spot area and $t_{\text{ref,nd}} = t_{\text{ref}} \dfrac{K\mu^2}{\rho C_p}$ the non-dimensional reflex time as defined in subsection 6.1. As the beam spot area A_{nd} increases, we expect the reflex time $t_{\text{ref,nd}}$ decrease to a positive value above zero. Thus, for $t_{\text{ref,nd}}$, we seek an expansion of the form:

$$t_{\text{ref,nd}}(A_{\text{nd}}) = t_0 \left[1 + c_A \left(\frac{1}{A_{\text{nd}}} \right)^{\alpha} + \cdots \right] \tag{29}$$

Substituting expansion form (29) into Equation (28) and carrying out the Taylor expansion of $H(\Delta y, t_0 + \Delta t)$ around $(0, t_0)$, we get

$$\frac{(T_{\text{act}} - T_0)K\mu}{P_{\text{dep}}} = H(0, t_0) + \frac{\partial H(0, t_0)}{\partial t}\left(t_{\text{ref,nd}}(A_{\text{nd}}) - t_0 \right)$$
$$+ \left. \frac{\partial H(y, t_0)}{\partial y} \right|_{y=0} \left(\frac{1}{A_{\text{nd}}} \right) + \frac{1}{2} \left. \frac{\partial^2 H(y, t_0)}{\partial y^2} \right|_{y=0} \left(\frac{1}{A_{\text{nd}}} \right)^2 \tag{30}$$

Based on governing Equation (20) and expression (22) of $H(y,t)$, we can derive:

$$h(t) \equiv H(0, t) = \text{erfc}\left(\sqrt{t} \right) e^t - 1 + \frac{2}{\sqrt{\pi}} \sqrt{t} \tag{31}$$

$$\frac{\partial H(0, t)}{\partial t} = \text{erfc}\left(\sqrt{t} \right) e^t, \quad \left. \frac{\partial H(y, t)}{\partial y} \right|_{y=0} = 0$$

$$\left. \frac{\partial^2 H(y, t)}{\partial y^2} \right|_{y=0} = \text{erfc}\left(\sqrt{t} \right) e^t - 1$$

Using these results in expansion (30), we obtain

$$\frac{\left(T_{\text{act}}-T_0\right)K\mu}{P_{\text{dep}}}$$

$$=h\left(t_0\right)+\text{erfc}\left(\sqrt{t_0}\right)e^{t_0}t_0 c_A\left(\frac{1}{A_{\text{nd}}}\right)^\alpha+\frac{1}{2}\left(\text{erfc}\left(\sqrt{t_0}\right)e^{t_0}-1\right)\left(\frac{1}{A_{\text{nd}}}\right)^2 \tag{32}$$

Matching corresponding terms of $\left(\dfrac{1}{A_{\text{nd}}}\right)$ on both sides of (32) yields

$$h\left(t_0\right)=\frac{\left(T_{\text{act}}-T_0\right)K\mu}{P_{\text{dep}}},\ \ \alpha=2,$$

$$\text{and}\ \ \text{erfc}\left(\sqrt{t_0}\right)e^{t_0}t_0 c_A+\frac{1}{2}\left(\text{erfc}\left(\sqrt{t_0}\right)e^{t_0}-1\right)=0 \tag{33}$$

Using expansion (29) and $\alpha=2$, we write out the expansion of the physical reflex time.

Case B: with heat conduction

$$t_{\text{ref}}\left(A\right)=\frac{\rho C_p}{K\mu^2}t_0\left[1+c_A\left(\frac{\mu z_c}{A}\right)^2+\cdots\right] \tag{34}$$

where t_0 and c_A are solved from (33) and are given by

$$\begin{cases} t_0 = h^{-1}\left(\dfrac{\left(T_{\text{act}}-T_0\right)K\mu}{P_{\text{dep}}}\right) \\[4mm] c_A = \dfrac{1-\text{erfc}\left(\sqrt{t_0}\right)e^{t_0}}{2\,\text{erfc}\left(\sqrt{t_0}\right)e^{t_0}t_0} \end{cases} \tag{35}$$

Here $h^{-1}(\cdot)$ denotes the inverse function of $h(t)$ defined in (31). We compare (13) and (34). The reflex time in (34) converges rapidly to a positive value above zero as the beam spot area A increases. The convergence of $1/A^2$ in (34) (the case with heat conduction) is faster than the convergence of $1/A$ in (13) (the case of no heat conduction).

7.2. Latency in Withdrawal Reflex

We study the behavior of biological latency (time delay) t_{del} in observed reflex in case B (the case with heat conduction). We investigate the mathematical formulation for determining t_{del} from test data. While the true reflex time varies with the applied power density P_{dep} and with the beam spot area A, we assume that the time delay in observed reflex is an intrinsic property of the test subject and is independent of P_{dep} and A. In experiments, applied power density P_{dep} and beam spot area A are adjustable. Our strategy is to determine the time delay t_{del} using observed reflex times at a sequence of P_{dep} values.

The observed reflect time is the sum of the true reflex time and the unknown time delay: $t_{\text{obs}}=t_{\text{ref}}+t_{\text{del}}$. As a function of beam spot area A, the true reflex time t_{ref} has expansion (34). At large non-dimensional $\dfrac{A}{\mu z_c}$, the observed ref-

lex time t_{obs} is approximately

$$t_{obs} = t_{ref} + t_{del} \approx \frac{\rho C_p}{K\mu^2} h^{-1}\left(\frac{(T_{act} - T_0)K\mu}{P_{dep}} \right) + t_{del} \tag{36}$$

In the limit of $\dfrac{A}{\mu z_c} \to \infty$, the observed reflex time t_{obs} as a function of P_{dep} has the form:

$$t_{obs}(P_{dep}) = c_1 h^{-1}\left(\frac{c_2}{P_{dep}} \right) + t_{del} \tag{37}$$

$$c_2 \equiv (T_{act} - T_0)K\mu, \quad c_1 \equiv \frac{\rho C_p}{K\mu^2}$$

In (37), besides the unknown time delay t_{del}, the two coefficients c_1 and c_2 are also unknown while P_{dep} is specified in experiments. We want to estimate t_{del} from measurements of t_{obs} vs P_{dep}. Notice that the three unknowns (c_2, c_1, t_{del}) and measurable quantities (P_{dep}, t_{obs}) are constrained by a parameter-free function $h^{-1}(u)$ in Equation (37). This mathematical observation suggests an approach for determining t_{del}:

- measure three data points of (P_{dep}, t_{obs}), and use formulation (37) to construct three constraint equations for (c_2, c_1, t_{del}) based on the three measured data points;
- then solve for (c_2, c_1, t_{del}) simultaneously from the system of joint constraints.

Specifically, we carry out tests at 3 values of P_{dep}:

$$P_{dep} = p_0, \quad P_{dep} = 2p_0, \quad P_{dep} = 4p_0$$

We examine the difference in the observed reflex time. The difference is independent of t_{del}.

$$t_{obs}(p_0) - t_{obs}(2p_0) = c_1\left[h^{-1}\left(\frac{c_2}{p_0} \right) - h^{-1}\left(\frac{c_2}{2p_0} \right) \right] \tag{38}$$

$$t_{obs}(2p_0) - t_{obs}(4p_0) = c_1\left[h^{-1}\left(\frac{c_2}{2p_0} \right) - h^{-1}\left(\frac{c_2}{4p_0} \right) \right] \tag{39}$$

In (38) and (39), the number of unknowns is reduced to two: c_1 and c_2. Next, we get rid of unknown c_1. For that purpose, we consider quantity v_{obs} defined as

$$v_{obs} \equiv \frac{(t_{obs}(p_0) - t_{obs}(2p_0)) - 2(t_{obs}(2p_0) - t_{obs}(4p_0))}{(t_{obs}(p_0) - t_{obs}(2p_0)) + 2(t_{obs}(2p_0) - t_{obs}(4p_0))} \tag{40}$$

From (38) and (39), it follows that v_{obs} is a function of c_2/p_0

$$v_{obs} = R\left(\frac{c_2}{p_0} \right) \tag{41}$$

where function $R(u)$ is defined in terms of $h^{-1}(\cdot)$ as

$$R(u) \equiv \frac{\left(h^{-1}(u) - h^{-1}(u/2)\right) - 2\left(h^{-1}(u/2) - h^{-1}(u/4)\right)}{\left(h^{-1}(u) - h^{-1}(u/2)\right) + 2\left(h^{-1}(u/2) - h^{-1}(u/4)\right)} \tag{42}$$

Function $h(t)$ is defined in (31) and is parameter-free. As a result, function $R(u)$ introduced above is also parameter-free. **Figure 4** demonstrates that $R(u)$ is an increasing function. This observation indicates that the inverse function $R^{-1}(\cdot)$ is well defined.

In **Appendix C**, we derive asymptotics of $R(u)$. The asymptotic results are

$$\begin{cases} R(u) = \dfrac{5 - 3\sqrt{2}}{3\sqrt{\pi}} u^{1/2} + \left(\dfrac{4\sqrt{2}}{9\pi} - \dfrac{3}{16}\right) u + \cdots & \text{for small } u \\[4mm] R(u) = \dfrac{1}{3}\left[1 - \dfrac{16}{9u} + \dfrac{16^2}{9^2 u^2} + \cdots\right] & \text{for large } u \end{cases} \tag{43}$$

These asymptotic results establish analytically the invertibility of function $R(u)$ in the region of small u and in the region of large u. The invertibility of $R(u)$ allows the calculation of c_2 in Equation (41), which subsequently leads to the determination of t_{del}.

We now describe the method of determining t_{del} from data of t_{obs} vs P_{dep}. Given three data points of observed reflex time vs. power density: $t_{\text{obs}}(p_0)$, $t_{\text{obs}}(2p_0)$ and $t_{\text{obs}}(4p_0)$, we proceed as follows. We first calculate quantity v_{obs} as described in (40). Then we apply the inverse function $R^{-1}(\cdot)$ to both sides of (41) to find c_2. Next we substitute the obtained value of c_2 into (38) to calculate c_1. Finally, with the values of c_2 and c_1, we calculate t_{del} in (37). Mathematically we write the method as an algorithm:
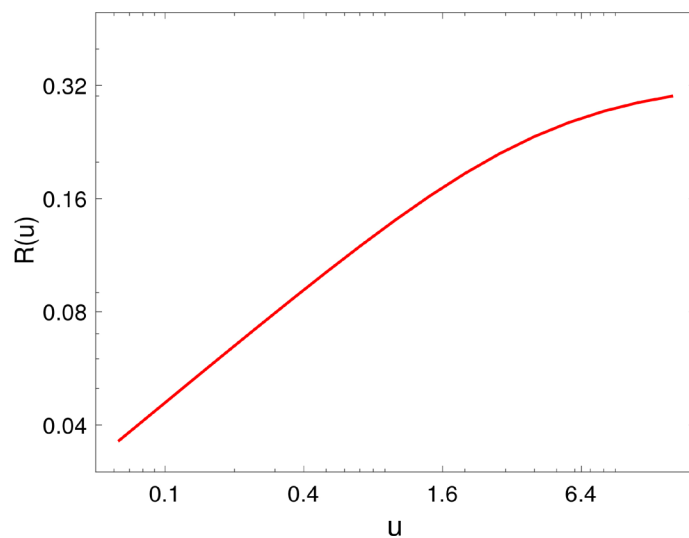
Case B: with heat conduction

Figure 4. Graph of function $R(u)$ shows it increases monotonically with *u*.

$$\begin{cases} v_{\text{obs}} \text{ is calculated from data using } (40) \\ c_2^{(\text{est})} = p_0 R^{-1}\left(v_{\text{obs}}\right) \\ c_1^{(\text{est})} = \dfrac{t_{\text{obs}}\left(p_0\right) - t_{\text{obs}}\left(2p_0\right)}{h^{-1}\left(c_2^{(\text{est})}/p_0\right) - h^{-1}\left(c_2^{(\text{est})}/\left(2p_0\right)\right)} \\ t_{\text{del}}^{(\text{est})} = t_{\text{obs}}\left(p_0\right) - c_1^{(\text{est})} h^{-1}\left(c_2^{(\text{est})}/p_0\right) \\ t_{\text{obs}}^{(\text{pred})}\left(P_{\text{dep}}\right) = c_1^{(\text{est})} h^{-1}\left(\dfrac{c_2^{(\text{est})}}{P_{\text{dep}}}\right) + t_{\text{del}}^{(\text{est})} \end{cases} \tag{44}$$

The last line of (44) gives the predicted function of observed reflex time vs. applied power density, based on the 3 data points. Algorithm (44) is parameter-free. It calculates the time delay t_{del} using only the 3 data points. Even though algorithm (44) is derived based on the theoretical behavior of case B in the limit of large beam spot area, operationally it can be applied in any situation since it does not require any input parameter. In the next section, we will test it in the case of a Gaussian beam where the temperature is not uniform over the beam cross-section and the beam radius is finite.

7.3. Temperature at a Fixed Depth for Small Time and Large Time

In this subsection, we study the time evolution of the normalized non-dimensional temperature $H(y,t)$ at a fixed y, respectively for small t and for large t. Here the pair (y,t) denotes the non-dimensional depth and time. $H(y,t)$ is governed by Equation (20). We will see that over short time, the temperature increase caused by the heating term in (20) is augmented by the heat gain via conduction. Over long time, however, the effect of the heating term is very much diminished by the heat loss via conduction.

In solution (22), $H(y,t)$ is an integral of $G(y,t)$. We first look at the asymptotics of $G(y,t)$. At a fixed $y > 0$, as $G(y,t)$ we have $\dfrac{y}{\sqrt{t}} \to +\infty$. Recall two properties of $\text{erfc}(\cdot)$:

$$\text{erfc}(z) = 0 + \text{T.S.T.} \quad \text{as } z \to +\infty$$

$$\text{erfc}(-z) = 2 + \text{T.S.T.} \quad \text{as } z \to +\infty$$

The abbreviation T.S.T stands for Transcendentally Small Terms, which converge to zero faster than any powers of *z*. At a fixed $y > 0$ and small *t*, we use these two properties to calculate the expansions of $G(y,t)$ and $H(y,t)$ in (22).

$$G(y,t) = e^{t-y} + \text{T.S.T.} \quad \text{for small } t$$

$$H(y,t) = \int_0^t G(y,s)\,ds = e^{-y}\left(e^t - 1\right) + \text{T.S.T.} \quad \text{for small } t \tag{45}$$

In the no-conduction approximation given in (25), $H_0(y,t) = te^{-y}$ is proportional to *t* for all *t*. The increase rate of $H_0(y,t)$ is independent of *t*. With heat conduction, the solution $H(y,t)$ increases slightly more than linearly with

t in (45) for small t.

$$\left(e^{t}-1\right)=\left(t+\frac{1}{2}t^{2}+\cdots\right)>t$$

The linear portion of the temperature growth at depth y is attributed to the heating at y from the electromagnetic wave penetrating into the skin. The portion above the linear growth is caused by the positive net heat gain via conduction. For a small interval around y, the net heat gain via conduction is positive when the heat in-flow from the upstream is more than the heat out-flow to the downstream. The temperature growth caused by the electromagnetic heating is augmented by the conduction when the net heat gain via conduction is positive. Mathematically, at depth y, the net heat gain via conduction is positive when $\partial^{2}H(y,t)/\partial^{2}y>0$, which is true for small t. We will show below that for large t, however, the net heat gain via conduction is negative. As a result, the temperature increase caused by electromagnetic heating is diminished by heat conduction, and the realized temperature increase for large t is much smaller than the linear growth.

To expand $G(y,t)$ for large t, we write it in terms of the scaled complementary error function $\operatorname{erfcx}(z)\equiv\operatorname{erfc}(z)\exp(z^{2})$.

$$G(y,t)=\frac{1}{2}\left(\left.\operatorname{erfcx}(z)\right|_{z=\sqrt{t}-\frac{y}{2\sqrt{t}}}+\left.\operatorname{erfcx}(z)\right|_{z=\sqrt{t}+\frac{y}{2\sqrt{t}}}\right)\exp\left(\frac{-y^{2}}{4t}\right)$$

We use the expansion of $\operatorname{erfcx}(z)$ given in (68) of **Appendix C**.

$$G(y,t)=\frac{1}{\sqrt{\pi}\sqrt{t}}\left(1-\frac{2+y^{2}}{4t}+\cdots\right)\quad\text{for large }t \tag{46}$$

Integrating the expansion of $G(y,t)$ with respect to t, we obtain

$$H(y,t)=\frac{2}{\sqrt{\pi}}t^{1/2}+c_{0}(y)+\frac{2+y^{2}}{2\sqrt{\pi}}t^{-1/2}+\cdots\quad\text{for large }t \tag{47}$$

The constant term $c_{0}(y)$ is undetermined in the integration. In **Appendix D**, we derive $c_{0}(y)=-\left(e^{-y}+y\right)$. For large t, $H(y,t)$ increases like $\sqrt{t}$, much slower than the linear growth in the no-conduction approximation $H_{0}(y,t)=te^{-y}$. The effect of the heating term in (20) is very much neutralized by the net heat loss at y via conduction. This slow temperature increase at large t is in sharp contrast with the situation for small t where the effect of the heating term is augmented by the net heat gain via conduction. Of course, heat is conserved in the conduction. The net heat loss at depth y_{1} contributes to a potential net heat gain somewhere downstream (at depth $y_{2}>y_{1}$). Expansions (46) and (47) are based on $z=\sqrt{t}\left(1-\frac{y}{2t}\right)\to+\infty$. The qualification of "large t" depends on the value of y. At any fixed t (no matter how large it is), when y is large enough, eventually $z=\sqrt{t}\left(1-\frac{y}{2t}\right)$ is negative, and expansions (46) and (47) are invalid. In the regime of fixed t and large y, the net heat gain at y via conduc-

tion is positive. Expansions (46) and (47), however, tell us the behavior in a different regime: at a fixed $y > 0$, when t is large enough, the electromagnetic heating is diminished by the net heat loss via conduction and it produces a much slower temperature growth proportional to $\sqrt{t}$ instead of t.

We compare the normalized temperature $H(y,t)$, its asymptotics for small t and for large t, and the no-conduction approximation $H_0(y,t)$. We like to compare them in their relative differences over a wide range of time t. Given that $H_0(y,t)$ is proportional to t, we scale everything by $1/t$ to facilitate the comparison. $H(y,t)/t$ has the physical meaning of the average rate of temperature increase in $[0,t]$. Figure 5 shows the scaled exact solution $H(y,t)/t$, its asymptotic approximations (45) for small t and (47) and for large t, and the scaled no-conduction approximation $H_0(y,t)/t = e^{-y}$.

We look into the net heat gain/loss due to conduction, for small t and for large t. Differentiating (45) and (47) twice with respect to y, we have

$$\text{Net heat gain}: \frac{\partial^2 H}{\partial y^2} = \begin{cases} e^{-y}\left(e^t - 1\right) > 0 & \text{for small } t \\ -e^{-y} + \dfrac{1}{\sqrt{\pi}}t^{-1/2} < 0 & \text{for large } t \end{cases} \tag{48}$$

The results in (48) are valid only when (45) and (47) are valid, respectively, in the regimes of small t and large t. This is particularly evident in line 2 of (48), which suggests that at fixed depth y, the regime of large t has to satisfy $t > e^{2y}/\pi$. Since there is no heat in-flow at depth 0 (skin surface), the conduction always leads to an overall heat loss for the interval $[0, y]$. The local net heat loss is initially confined to near 0 and gradually propagates to the entire interval. For large y, it takes long time for the local net heat loss to reach depth y. It takes even longer time for the net heat loss to offset the previously accumulated heat gain at y and then to substantially neutralize the electromagnetic heating.
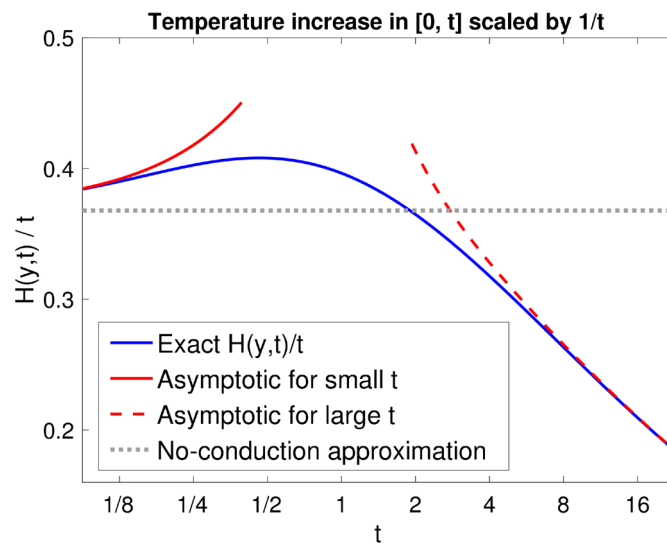

Figure 5. $H(y,t)/t$, its asymptotics (45) and (47), and no-conduction approximation $H_0(y,t)/t$, over a wide range of time t. Parameter used: $y = 1$ (non-dimensional).

7.4. Reflex Times at Large and at Small Applied Power Densities

In case B, the temperature is uniform over the beam cross section and the activated region is a cylinder. Given the beam spot area A and the threshold z_c for activated volume, withdrawal reflex occurs when the temperature at depth z_c/A reaches the activation temperature T_{act}. In this subsection, we use the asymptotics of temperature for small time and for large time (obtained in subsection 7.3) to study the reflex time at large and at small applied power densities. We also compare the results with the no-conduction approximation of the reflex time given in (10), which is inversely proportional to the applied power density.

In case B, the reflex time t_{ref} satisfies equation $T\left(z_c/A, t_{\text{ref}}\right) = T_{\text{act}}$, as described in (8). The non-dimensional version of the equation is given in (28). For our discussion here, we write the left side of (28) in terms of $T_{\text{act,nd}}$ and $P_{\text{dep,nd}}$.

$$H\left(\frac{1}{A_{\text{nd}}}, t_{\text{ref,nd}}\right) = \frac{T_{\text{act,nd}}}{P_{\text{dep,nd}}} \tag{49}$$

where $H(y,t)$ is the parameter-free normalized non-dimensional temperature defined in (22). We consider the function of $t_{\text{ref,nd}}$ vs $P_{\text{dep,nd}}$ and denote it concisely as $\tau\left(P_{\text{dep,nd}}\right)$.

The no-conduction version of Equation (49) is obtained by replacing $H(y,t)$ with its no-conduction approximation $H_0(y,t) = t\mathrm{e}^{-y}$. The solution of the no-conduction version of (49) gives the no-conduction approximation of $\tau\left(P_{\text{dep,nd}}\right)$

Case A: no heat conduction

$$\tau^{(0)}\left(P_{\text{dep,nd}}\right) = \frac{T_{\text{act,nd}}}{P_{\text{dep,nd}}}\mathrm{e}^{1/A_{\text{nd}}} \propto \frac{1}{P_{\text{dep,nd}}} \tag{50}$$

For large $P_{\text{dep,nd}}$, we expect small $\tau\left(P_{\text{dep,nd}}\right)$, we use the asymptotic for small t given in (45) to approximate $H(y,t)$, and we write Equation (49) approximately as

$$\mathrm{e}^{-1/A_{\text{nd}}}\left(\mathrm{e}^{\tau} - 1\right) = \frac{T_{\text{act,nd}}}{P_{\text{dep,nd}}} \quad \text{for large } P_{\text{dep,nd}}$$

which yields

$$\begin{aligned}
\tau\left(P_{\text{dep,nd}}\right) &= \ln\left(1 + \frac{T_{\text{act,nd}}}{P_{\text{dep,nd}}}\mathrm{e}^{1/A_{\text{nd}}}\right) \quad \text{for large } P_{\text{dep,nd}} \\
&= \tau^{(0)}\left(P_{\text{dep,nd}}\right)\left(1 - \frac{T_{\text{act,nd}}}{P_{\text{dep,nd}}}\mathrm{e}^{1/A_{\text{nd}}} + \cdots\right)
\end{aligned} \tag{51}$$

Result (51) indicates that heat conduction reduces the reflex time when the applied power density is large. This corresponds to the asymptotic result in subsection 7.3 that at a fixed depth and over short time, heat conduction enhances the temperature increase of electromagnetic heating. We measure the relative reduction in reflex time by

$$\frac{\tau^{(0)}\left(P_{\mathrm{dep,nd}}\right) - \tau\left(P_{\mathrm{dep,nd}}\right)}{\tau^{(0)}\left(P_{\mathrm{dep,nd}}\right)} = \frac{T_{\mathrm{act,nd}}}{P_{\mathrm{dep,nd}}} \mathrm{e}^{1/A_{\mathrm{nd}}} + \cdots$$

The relative reduction in reflex time actually increases slightly when the applied power density is slightly decreased as long as it is still in the regime of large power density so that the small time approximation (45) is valid.

For small $P_{\mathrm{dep,nd}}$, we expect large $\tau\left(P_{\mathrm{dep,nd}}\right)$, we use asymptotic for large t given in (47) to approximate $H(y,t)$, and we write Equation (49) approximately as

$$\frac{2}{\sqrt{\pi}}\tau^{1/2} - \left(\mathrm{e}^{-1/A_{\mathrm{nd}}} + 1/A_{\mathrm{nd}}\right) + \frac{2 + \left(1/A_{\mathrm{nd}}\right)^2}{2\sqrt{\pi}}\tau^{-1/2} = \frac{T_{\mathrm{act,nd}}}{P_{\mathrm{dep,nd}}}$$

which becomes a quadratic equation for $\sqrt{\tau}$ and gives the solution

$$\tau\left(P_{\mathrm{dep,nd}}\right) = \left(\frac{b_1 + \sqrt{b_1^2 - \left(2 + \left(1/A_{\mathrm{nd}}\right)^2\right)}}{2}\right)^2 \quad \text{for small } P_{\mathrm{dep,nd}} \qquad (52)$$

$$b_1 = \frac{\sqrt{\pi}}{2}\left(\frac{T_{\mathrm{act,nd}}}{P_{\mathrm{dep,nd}}} + \mathrm{e}^{-1/A_{\mathrm{nd}}} + 1/A_{\mathrm{nd}}\right)$$

The second solution of the quadratic equation satisfies $\lim_{P_{\mathrm{dep,nd}} \to 0} \tau\left(P_{\mathrm{dep,nd}}\right) = 0$, which is unreasonable. The expansion of (52) as a power series of $P_{\mathrm{dep,nd}}$ is

$$\tau\left(P_{\mathrm{dep,nd}}\right) = \frac{\pi T_{\mathrm{act,nd}}^2}{4 P_{\mathrm{dep,nd}}^2}\left[1 + a_1 \frac{P_{\mathrm{dep,nd}}}{T_{\mathrm{act,nd}}} + a_2 \frac{P_{\mathrm{dep,nd}}^2}{T_{\mathrm{act,nd}}^2} + \cdots\right] \quad \text{for small } P_{\mathrm{dep,nd}} \qquad (53)$$

$$a_1 = 2\left(\mathrm{e}^{\frac{-1}{A_{\mathrm{nd}}}} + \frac{1}{A_{\mathrm{nd}}}\right), \quad a_2 = \left(\mathrm{e}^{\frac{-1}{A_{\mathrm{nd}}}} + \frac{1}{A_{\mathrm{nd}}}\right)^2 - \frac{2}{\pi}\left(2 + \frac{1}{A_{\mathrm{nd}}^2}\right)$$

Result (53) indicates that for small applied power density $P_{\mathrm{dep,nd}}$, the reflex time $t_{\mathrm{ref,nd}}$ increases enormously, proportional to $\left(1/P_{\mathrm{dep,nd}}\right)^2$ instead of proportional to $1/P_{\mathrm{dep,nd}}$. This corresponds to the asymptotic result in subsection 7.3 that at a fixed depth and over long time, heat conduction results in local net heat loss and significantly diminishes the temperature increase of electromagnetic heating.

We compare reflex times $\tau\left(P_{\mathrm{dep,nd}}\right)$, the two asymptotics and $\tau^{(0)}\left(P_{\mathrm{dep,nd}}\right)$. As $P_{\mathrm{dep,nd}}$ increases, $\tau\left(P_{\mathrm{dep,nd}}\right)$ varies extensively from being extremely large at small $P_{\mathrm{dep,nd}}$ to being near zero at large $P_{\mathrm{dep,nd}}$. To examine the relative differences over a wide range of $P_{\mathrm{dep,nd}}$, we scale everything by $P_{\mathrm{dep,nd}}$ to reduce their variations with $P_{\mathrm{dep,nd}}$. In particular, after scaling, $\tau^{(0)}\left(P_{\mathrm{dep,nd}}\right)P_{\mathrm{dep,nd}} = T_{\mathrm{act,nd}}\mathrm{e}^{1/A_{\mathrm{nd}}}$ is independent of $P_{\mathrm{dep,nd}}$. Physically, $\tau\left(P_{\mathrm{dep,nd}}\right)P_{\mathrm{dep,nd}}$ has the meaning of energy deposited per area on skin by the time of reflex. When the beam spot area is fixed, $\tau\left(P_{\mathrm{dep,nd}}\right)P_{\mathrm{dep,nd}}$ can be used as a measure of energy consumption by the time of reflex. Figure 6 compares the exact solution $\tau\left(P_{\mathrm{dep,nd}}\right)P_{\mathrm{dep,nd}}$, its asymptotic approximations (51) for large $P_{\mathrm{dep,nd}}$ and (52) and for small $P_{\mathrm{dep,nd}}$, and the no-conduction approximation $\tau^{(0)}\left(P_{\mathrm{dep,nd}}\right)P_{\mathrm{dep,nd}}$.
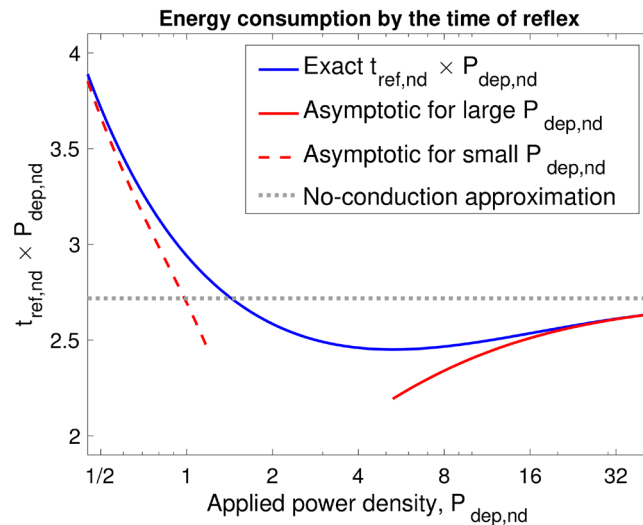
Figure 6. $\tau\left(P_{\text{dep,nd}}\right)P_{\text{dep,nd}}$, its asymptotics (52) and (51), and no-conduction approximation $\tau^{(0)}\left(P_{\text{dep,nd}}\right)P_{\text{dep,nd}}$. Parameters used: $T_{\text{act,nd}}=1$ and $A_{\text{nd}}=1$.

In **Figure 6**, we make an important observation that the energy consumption has a minimum with respect to applied power density. We now demonstrate the minimum analytically. Based on asymptotics (51) and (53), $\tau\left(P_{\text{dep,nd}}\right)P_{\text{dep,nd}}$ has the expansions below, respectively, for small $P_{\text{dep,nd}}$ and for large $P_{\text{dep,nd}}$

$$\tau\left(P_{\text{dep,nd}}\right)P_{\text{dep,nd}} = \begin{cases} T_{\text{act,nd}}\mathrm{e}^{1/A_{\text{nd}}}\left(1-\dfrac{T_{\text{act,nd}}}{P_{\text{dep,nd}}}\mathrm{e}^{1/A_{\text{nd}}}\right) & \text{for large } P_{\text{dep,nd}} \\[2em] \dfrac{\pi T_{\text{act,nd}}^2}{4P_{\text{dep,nd}}} & \text{for small } P_{\text{dep,nd}} \end{cases} \tag{54}$$

For large $P_{\text{dep,nd}}$, $\tau\left(P_{\text{dep,nd}}\right)P_{\text{dep,nd}}$ approaches its no-conduction approximation $T_{\text{act,nd}}\mathrm{e}^{1/A_{\text{nd}}}$ from below; for small $P_{\text{dep,nd}}$, $\tau\left(P_{\text{dep,nd}}\right)P_{\text{dep,nd}}$ grows unbounded. The minimum of $\tau\left(P_{\text{dep,nd}}\right)P_{\text{dep,nd}}$ is attained in between when $P_{\text{dep,nd}}$ is moderately large. In general, the range of moderately large $P_{\text{dep,nd}}$ is also a good compromise between inducing withdrawal reflex quickly and preventing burn injury of accidental over-heating. For large $P_{\text{dep,nd}}$, burn injury may occur even when the power is turned off shortly after the internal initiation of withdrawal reflex.

7.5. Spatial Temperature Profile at Reflex

We examine the temperature profile at reflex and how it varies as the applied power density increases from small to large. We compare it with the no-conduction approximation, which is independent of the applied power density.

We follow the equation and notation for the reflex time used in subsection 7.4. At reflex, the non-dimensional temperature has the expression

$$\text{Temperature at reflex}: \begin{cases} T_{\text{nd}}\left(y_{\text{nd}}\right)\big|_{\text{reflex}} = P_{\text{dep,nd}}H\left(y_{\text{nd}},\tau\right) \\[1em] \tau \text{ is the solution of } H\left(\dfrac{1}{A_{\text{nd}}},\tau\right)=\dfrac{T_{\text{act,nd}}}{P_{\text{dep,nd}}} \end{cases} \tag{55}$$

The no-conduction approximation of $H(y,t)$ is $H_0(y,t) = te^{-y}$, which has separable dependence on t and y. The no-conduction approximation of (55) is

$$\text{No-conduction approximation}: T_{\text{nd}}^{(0)}(y_{\text{nd}})\big|_{\text{reflex}} = T_{\text{act,nd}}\exp\left(\frac{1}{A_{\text{nd}}} - y_{\text{nd}}\right)$$

which is independent of the applied power density $P_{\text{dep,nd}}$. In the presence of heat conduction, the normalized temperature $H(y,t) = \int_0^t G(y,s)\,\mathrm{d}s$ has non-separable dependence on t and y. Consequently, $T_{\text{nd}}(y_{\text{nd}})\big|_{\text{reflex}}$ in (55) varies with $P_{\text{dep,nd}}$. **Figure 7** compares $T_{\text{nd}}(y_{\text{nd}})\big|_{\text{reflex}}$ for several values of $P_{\text{dep,nd}}$ and its no-conduction approximation. As $P_{\text{dep,nd}}$ increases, the reflex time decreases to zero, and the heat conduction has little time to take its effect. **Figure 7** demonstrates that at a fixed depth $y > 0$, as $P_{\text{dep,nd}}$ increases the temperature at reflex converges to that in the case of no heat conduction. Therefore, at any fixed depth away from the skin surface, the effect of heat conduction is eventually negligible when the applied power density is large enough.

7.6. Selecting Test Conditions for Determining (T_{act}, z_c)

The situation of inferring parameters (T_{act}, z_c) from temperature profiles at t_{ref} is similar to that in the case of no heat conduction. Once the latency t_{del} is determined, the true reflex time is calculated from the observed reflex time: $t_{\text{ref}} = t_{\text{obs}} - t_{\text{del}}$. Given the temperature profile at reflex $T(r, y, t_{\text{ref}})$ at one test condition, the activation temperature T_{act} can be set to any value in the range of $T(r, y, t_{\text{ref}})$. At each value of T_{act}, the corresponding threshold $z_c(T_{\text{act}})$ is calculated as the activated volume at reflex according to formula (5). When restricted to data at one test condition, $T(r, y, t_{\text{ref}})$ provides only one constraint on (T_{act}, z_c); it does not allow us to determine T_{act} and z_c simultaneously.

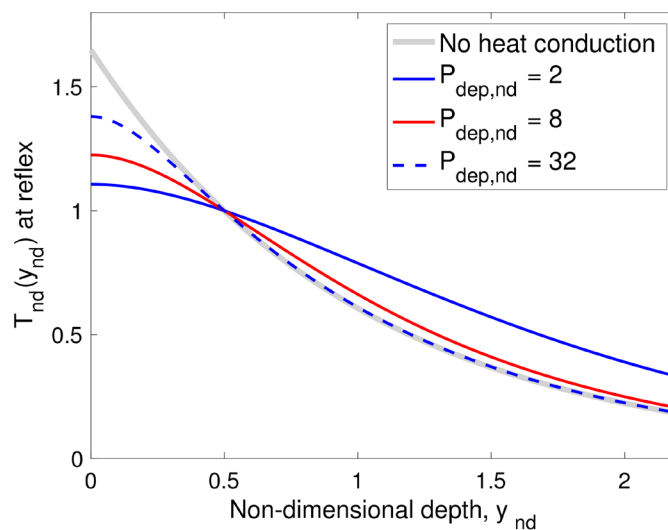As we discussed in section 4, constraint function $z_c(T_{\text{act}})$ is calculated

Figure 7. Non-dimensional temperature profile at reflex, $T_{\text{nd}}(y_{\text{nd}})\big|_{\text{reflex}}$, for various values of applied power density $P_{\text{dep,nd}}$. Parameters used: $T_{\text{act,nd}} = 1$, $A_{\text{nd}} = 2$.

directly from the measured temperature profile at reflex $T(\mathbf{r}, y, t_{\text{ref}})$. It does not require any model parameter, such as μ, K, or ρC_p. We explore how to obtain substantially distinct constraint equations for (T_{act}, z_c) by carrying out tests at different conditions. In case U (which includes both case A and case B), the activated region is a cylinder with the beam cross section as the base. Given the beam spot area A, the activated volume is completely specified by the activated depth. At reflex, the activated volume is z_c and the activated depth is z_c/A. In case B, the temperature has the analytical solution given in (22) and (23). When examining the constraint on (T_{act}, z_c) using the analytical solution, it is more convenient to view T_{act} as a function of z_c. For any positive value of z_c, the corresponding activation temperature $T_{\text{act}}(z_c)$ is given by the temperature at depth z_c/A, which leads to the constraint on (T_{act}, z_c) described in Equation (8).

The non-dimensional version of (8) is Equation (28). Recall that (28) was derived as the governing equation for the reflex time $t_{\text{ref,nd}}$ when other parameters including z_c and T_{act} are known and fixed. As an equation for $t_{\text{ref,nd}}$, the meaning of (28) is clear. In the situation of inferring (z_c, T_{act}), reflex time t_{ref} is known (from data) and we view (28) as a constraint equation on (z_c, T_{act}), with z_c as the independent variable and T_{act} the dependent variable. In this view, we need to be careful about the precise meaning of various terms in (28). In particular, the non-dimensional beam spot area $A_{\text{nd}} = \dfrac{A}{\mu z_c}$ varies with independent variable z_c, and thus is no longer a constant. To pinpoint the influence of independent variable z_c on various terms in (28), we use $(T_{\text{act}}^*, z_c^*)$ to denote the true value of (T_{act}, z_c), and introduce quantities below based on true values $(T_{\text{act}}^*, z_c^*)$.

$$A_{\text{nd}}^* = \frac{A}{\mu z_c^*}, \quad \Delta T^* = T_{\text{act}}^* - T_0, \quad P_{\text{dep,nd}}^* = P_{\text{dep}} \frac{1}{K\mu\Delta T^*}$$

For simplicity and clarity, we use τ to denote $t_{\text{ref,nd}}$ and write $1/A_{\text{nd}}$ as

$$\frac{1}{A_{\text{nd}}} = \frac{\mu z_c}{A} = \frac{\mu z_c^*}{A}\left(\frac{z_c^* + z_c - z_c^*}{z_c^*}\right) = \frac{1}{A_{\text{nd}}^*}\left(1 + \frac{z_c - z_c^*}{z_c^*}\right)$$

With the proper notations clarified above, we write constraint (28) as

$$\frac{T_{\text{act}} - T_0}{\Delta T^*} = P_{\text{dep,nd}}^* H\left(\frac{1}{A_{\text{nd}}^*}\left(1 + \frac{z_c - z_c^*}{z_c^*}\right), \tau\right) \tag{56}$$

The true value $(T_{\text{act}}^*, z_c^*)$ satisfies constraint (56). Subtracting the (56) evaluated at $(T_{\text{act}}^*, z_c^*)$ from the general (56), we write the constraint as

$$\frac{T_{\text{act}} - T_{\text{act}}^*}{\Delta T^*} = P_{\text{dep,nd}}^*\left[H\left(\frac{1}{A_{\text{nd}}^*}\left(1 + \frac{z_c - z_c^*}{z_c^*}\right), \tau\right) - H\left(\frac{1}{A_{\text{nd}}^*}, \tau\right)\right] \tag{57}$$

(57) is a constraint function in the form of $\dfrac{T_{\text{act}} - T_{\text{act}}^*}{\Delta T^*}$ vs $\dfrac{z_c - z_c^*}{z_c^*}$ and has

three parameters: $P_{dep,nd}^*$, A_{nd}^* and τ. The non-dimensional reflex time τ satisfies Equation (56) at $\left(T_{act}^*, z_c^*\right)$:

$$1 = P_{dep,nd}^* H\left(\frac{1}{A_{nd}^*}, \tau\right) \tag{58}$$

The solution τ is a function of $\left(P_{dep,nd}^*, A_{nd}^*\right)$. It follows that as a function of $\dfrac{T_{act} - T_{act}^*}{\Delta T^*}$ vs $\dfrac{z_c - z_c^*}{z_c^*}$, constraint (57) is completely determined once $\left(P_{dep,nd}^*, A_{nd}^*\right)$ is known.

We examine constraint (57) in the form of $\dfrac{T_{act} - T_{act}^*}{\Delta T^*}$ vs $\dfrac{z_c - z_c^*}{z_c^*}$ and explore the parameter space of $\left(P_{dep,nd}^*, A_{nd}^*\right)$. The purposes of adopting this form are i) to pinpoint the effect of $\left(P_{dep,nd}^*, A_{nd}^*\right)$; and ii) to focus on the shape of constraint functions relative to their intersection at $\left(T_{act}^*, z_c^*\right)$. As we discussed above, the relative shape is completely determined by $\left(P_{dep,nd}^*, A_{nd}^*\right)$, independent of other parameters. While this form is the proper mathematical tool for examining the behavior of constraint (57), we do need to point out that in real applications of inferring $\left(T_{act}^*, z_c^*\right)$ from test data, the form of $\dfrac{T_{act} - T_{act}^*}{\Delta T^*}$ vs $\dfrac{z_c - z_c^*}{z_c^*}$ is not operationally realistic since T_{act}^* and z_c^* are unknown to start with. In real applications, we simply calculate constraint function $z_c\left(T_{act}\right)$ from test data using (5), and then find $\left(T_{act}^*, z_c^*\right)$ at the intersection of two constraint curves.

Figure 8 compares constraint (57) in the form of $\dfrac{T_{act} - T_{act}^*}{\Delta T^*}$ vs $\dfrac{z_c - z_c^*}{z_c^*}$ at several test conditions. A combination of large beam spot A_{nd}^* and small power
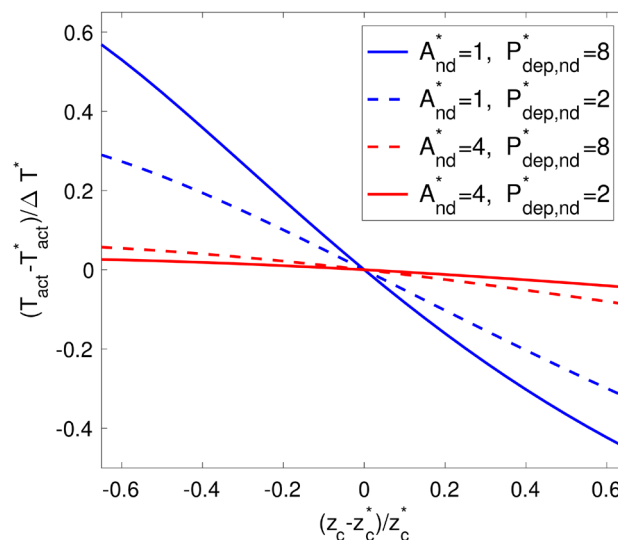

Figure 8. Constraints on $\left(T_{act}, z_c\right)$ in case B in the form of $\dfrac{T_{act} - T_{act}^*}{\Delta T^*}$ vs $\dfrac{z_c - z_c^*}{z_c^*}$. Different test conditions specified by $\left(P_{dep,nd}^*, A_{nd}^*\right)$ lead to distinct constraint curves.

density $P_{\text{dep,nd}}^{*}$ makes the constraint function flat while a combination of small A_{nd}^{*} and large $P_{\text{dep,nd}}^{*}$ makes it slate. Once we obtain two distinct constraints from different test conditions, the well-defined intersection of the two curves gives us the values of T_{act}^{*} and z_{c}^{*}.

In summary, to reliably determine model parameters T_{act}^{*} and z_{c}^{*}, we need to carry out tests with significantly different combinations of $\left(A_{\text{nd}}^{*}, P_{\text{dep,nd}}^{*}\right)$: one with moderate A_{nd}^{*} and large $P_{\text{dep,nd}}^{*}$, the other with large A_{nd}^{*} and moderate $P_{\text{dep,nd}}^{*}$.

8. The Case of a Gaussian Beam with Heat Conduction

We consider a Gaussian beam with power density

$$P_{\text{dep}}\left(\boldsymbol{r}\right) = P_{\text{dep}}^{(0)} \exp\left(\frac{-2|\boldsymbol{r}|^{2}}{w^{2}}\right) \tag{59}$$

where $P_{\text{dep}}^{(0)}$ is the power density at the beam center ($\boldsymbol{r} = 0$) and w is the beam radius, which is twice the standard deviation of the Gaussian distribution. At each value of $\boldsymbol{r}$, the temperature is governed by the electromagnetic heating and the heat conduction along the y-dimension, independent of the temperature at other values of $\boldsymbol{r}$. The temperature distribution $T\left(\boldsymbol{r}, y, t\right)$ is obtained by applying exact solution (23) at each $\boldsymbol{r}$

$$T\left(\boldsymbol{r}, y, t\right) = T_{0} + P_{\text{dep}}^{(0)} \exp\left(\frac{-2|\boldsymbol{r}|^{2}}{w^{2}}\right) \frac{1}{K\mu} H\left(\mu y, t \frac{K\mu^{2}}{\rho C_{p}}\right) \tag{60}$$

where $H\left(\cdot, \cdot\right)$ is the parameter-free normalized non-dimensional temperature defined in (22). The activated volume in spatial temperature profile (60) at a given time t does not have a closed-form expression. We use a numerical integration method to calculate the activated volume at any given time. The reflex time t_{ref} satisfies $\left(\text{activated volume}\right)\big|_{t_{\text{ref}}} = z_{c}$. We use an iterative non-linear solver to find t_{ref}. Once t_{ref} is known, we calculate $T\left(\boldsymbol{r}, y, t_{\text{ref}}\right)$ using (60). Following this procedure, we generate simulated data and then we use the data to test the theoretical predictions derived in the previous section for case B.

To facilitate the analysis, we introduce parameters c_{2} and c_{1} as in case B, and write temperature distribution (60) in a non-dimensional form, in terms of c_{2} and c_{1}.

$$\frac{T\left(\boldsymbol{r}, y, t\right) - T_{0}}{T_{\text{act}} - T_{0}} = \frac{P_{\text{dep}}^{(0)}}{c_{2}} \exp\left(\frac{-2|\boldsymbol{r}|^{2}}{w^{2}}\right) H\left(\mu y, \frac{t}{c_{1}}\right) \tag{61}$$

$$c_{2} \equiv \left(T_{\text{act}} - T_{0}\right) K\mu, \ c_{1} \equiv \frac{\rho C_{p}}{K\mu^{2}}.$$

8.1. Activated Domain and Reflex Time

First, we discuss how to generate simulated data of reflex time in the case of a Gaussian beam with finite radius. At time t, the activated domain is described by

$$D_{\text{activated}}(t) = \left\{ (\boldsymbol{r}, y) \big| T(\boldsymbol{r}, y, t) \geq T_{\text{act}} \right\}$$

$$= \left\{ (\boldsymbol{r}, y) \left| \frac{P_{\text{dep}}^{(0)}}{c_2} \exp\left(\frac{-2|\boldsymbol{r}|^2}{w^2} \right) H\left(\mu y, \frac{t}{c_1} \right) \geq 1 \right. \right\} \tag{62}$$

Figure 9 shows an example of activated domain for a Gaussian beam. Since the beam center ($r = 0$) has the highest intensity, near the beam center the skin receives more electromagnetic energy and the activated domain extends more in the depth direction. Away from the beam center, the beam intensity falls quickly and accordingly the depth of activated domain decreases toward 0. This leads to the bowl-shaped activated domain in **Figure 9**.

Withdrawal reflex occurs when the volume of the activated domain reaches the critical threshold z_c. The reflex time t_{ref} is governed by

$$\text{Volume} \left\{ (\boldsymbol{r}, y) \left| \exp\left(\frac{-2|\boldsymbol{r}|^2}{w^2} \right) H\left(\mu y, \frac{t_{\text{ref}}}{c_1} \right) \geq \frac{c_2}{P_{\text{dep}}^{(0)}} \right. \right\} = z_c \tag{63}$$

We non-dimensionalize spatial coordinates $\boldsymbol{r}$ and y, respectively with scales w and $1/\mu$.

$$\boldsymbol{r}_{\text{nd}} \equiv \frac{\boldsymbol{r}}{w}, \quad y_{\text{nd}} \equiv \mu y$$

Note that $\boldsymbol{r}$ and y are scaled differently. In coordinates $(\boldsymbol{r}_{\text{nd}}, y_{\text{nd}})$, (63) becomes

$$\text{Volume} \left\{ (\boldsymbol{r}_{\text{nd}}, y_{\text{nd}}) \left| \exp\left(-2|\boldsymbol{r}_{\text{nd}}|^2 \right) H\left(y_{\text{nd}}, \frac{t_{\text{ref}}}{c_1} \right) \geq \frac{c_2}{P_{\text{dep}}^{(0)}} \right. \right\} = \frac{\mu z_c}{w^2} \tag{64}$$

Equation (64) for t_{ref} is completely specified by parameters c_1, $c_2 / P_{\text{dep}}^{(0)}$ and $\mu z_c / w^2$. Function $H(y,t)$ is parameter-free and there is no other parameter. In simulations, we use

$$c_1 = 1, \quad c_2 = 1/2, \quad \mu z_c / w^2 = 1$$

With these parameters, we solve for the true reflex time t_{ref} from (64) as a function of $P_{\text{dep}}^{(0)}$. The observed reflex time is calculated as $t_{\text{obs}} = t_{\text{ref}} + t_{\text{del}}$. **Figure 10** plots the simulated function of t_{obs} vs $P_{\text{dep}}^{(0)}$ for a Gaussian beam. We
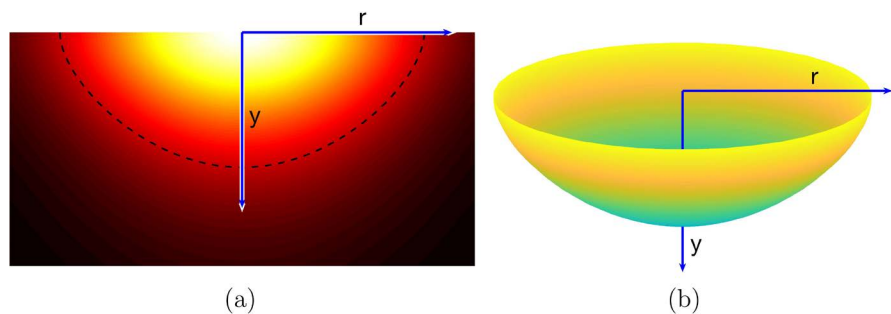

Figure 9. Activated domain in the case of a Gaussian beam. (a) Color map of $T(y,r)$ with the activated domain marked by dashed curve. (b) 3-D view of the activated domain.
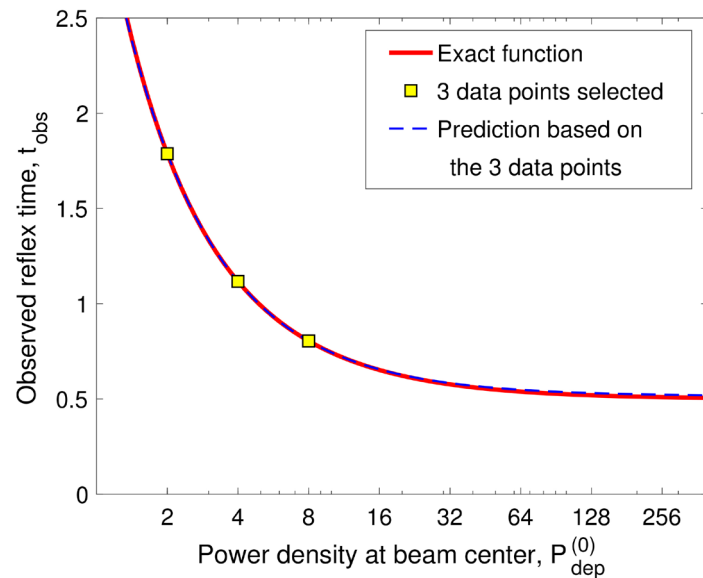
Figure 10. Observed reflex time t_{obs} vs beam center power density $P_{dep}^{(0)}$. Comparison of the simulated function (treated as exact) and the prediction by algorithm (44) based solely on the 3 data points shown above, without using any other information.

regard the simulated $t_{obs}\left(P_{dep}^{(0)}\right)$ in **Figure 10** as exact since it is numerically accurate to the computer precision.

8.2. Estimating the Latency

We study the methodology for determining the time delay in the observed withdrawal reflex: $t_{obs} = t_{ref} + t_{del}$. The time delay t_{del} is an intrinsic property of the test subject, independent of the applied power density $P_{dep}^{(0)}$. We estimate the time delay t_{del} based solely on the measured values of observed reflex time t_{obs}, without using any model parameters. In tests, $P_{dep}^{(0)}$ is tunable. The general strategy is to measure t_{obs} at a sequence of $P_{dep}^{(0)}$ values, and then use the test data to build multiple joint constraints on t_{del} and other unknowns. All parameters involved in the constraint formulation are treated as unknown, and all unknowns are solved simultaneously from the system of joint constraints.

In subsection 7.2, a joint constraint was constructed for 3 unknowns: t_{del}, c_2 and c_1. Equation (37) is derived in the idealized situation where.

- the applied power density is uniform over the beam cross-section and is zero outside; heat conduction is included in the depth direction (case B);
- the beam spot area is large and approaching infinity ($A \rightarrow \infty$).

Given 3 data points, we applied (37) to construct a constraint at each data point. Then we used the joint system of 3 constraints to derive algorithm (44) for determining t_{del}. Algorithm (44) is based solely on the 3 data points. It does not require any input parameter. In the idealized situation above, t_{del} solved from algorithm (44) is exact. In this subsection, we test the performance of algorithm (44) for inferring t_{del} in the case of a Gaussian beam with a finite beam radius. The purpose is to demonstrate the versatility and accuracy of algorithm (44)

when the idealized conditions above are not met. Here we focus on the accuracy of estimating the time delay since t_{del} is our objective while coefficients c_2 and c_1 are just auxiliary unknowns accompanying t_{del} in algorithm (44).

The simulated curve of t_{obs} vs $P_{dep}^{(0)}$ for a Gausian beam is shown in **Figure 10**. From the simulated curve, function values at $P_{dep}^{(0)} = p_0, 2p_0$ and $4p_0$ (with $p_0 = 2$) are selected as the 3 data points, shown as filled squares in **Figure 10**. These 3 data points and only these 3 data points are then used in algorithm (44) to estimate t_{del}. A Gaussian beam with finite beam radius does not satisfy the idealized conditions above. Nevertheless, we apply algorithm (44) to the 3 data points in **Figure 10** to estimate (c_2, c_1, t_{del}). Operationally, algorithm (44) is universally applicable in any situation since it does not require any input parameter.

Once we obtain the estimated values $\left(c_2^{(est)}, c_1^{(est)}, t_{del}^{(est)} \right)$, we use them in (44) to predict the observed reflex time as a function of $P_{dep}^{(0)}$.

$$t_{obs}^{(pred)}\left(P_{dep}^{(0)} \right) = c_1^{(est)} h^{-1} \left(\frac{c_2^{(est)}}{P_{dep}^{(0)}} \right) + t_{del}^{(est)}$$

Figure 10 demonstrates that the predicted function $t_{obs}^{(pred)}\left(P_{dep}^{(0)} \right)$ (dashed blue line) is a very good approximation of the exact function (solid red line). Note that the predicted function is based solely on the 3 data points. No other information is used.

8.3. Scaling Properties of the Formulation for Estimating Latency

In addition to its high accuracy for estimating the time delay in situations where the idealized conditions are not met, formulation (44) and the predicted function based on it, have several important properties. We now discuss these properties.

1) The prediction is based solely on the 3 data points. Formulation (44) and the predicted function $t_{obs}^{(pred)}\left(P_{dep}^{(0)} \right)$ are parameter-free. Coefficients c_2 and c_1 are auxiliary unknowns that are solved simultaneously with t_{del} in Equation (44).

2) The prediction is invariant with respect to a shift in t_{obs}. Quantity v_{obs} defined in (40) contains differences in observed reflex time among the 3 data points, and thus, is independent of time delay t_{del}. It follows that $c_2^{(est)}$ and $c_1^{(est)}$ calculated in (44) are independent of t_{del}. If the measured values of t_{obs} at 3 data points are shifted by a constant amount, then the estimated time delay $t_{del}^{(est)}$ and the predicted function $t_{obs}^{(pred)}\left(P_{dep}^{(0)} \right)$ are both shifted by the same amount. In other words, $\left(t_{del}^{(est)} - t_{del} \right)$ is invariant with respect to t_{del}. This can be seen by subtracting t_{del} in (44)

$$\left(t_{del}^{(est)} - t_{del} \right) = t_{ref}\left(p_0 \right) - c_1^{(est)} h^{-1} \left(c_2^{(est)} / p_0 \right)$$

In the equation above, all quantities on the right hand side are independent of t_{del}. Thus, the absolute error $\left(t_{del}^{(est)} - t_{del} \right)$ is not affected by t_{del}. The absolute error in $t_{del}^{(est)}$ reflects the model error that the Gaussian beam does not satisfy

the idealized conditions described in subsection 8.2. In **Figure 10**, the absolute error is $\left(t_{del}^{(est)} - t_{del}\right) = 0.014$, In data generation, we used $t_{del} = 0.5$. If we used a different value for t_{del}, it would not change the absolute error $\left(t_{del}^{(est)} - t_{del}\right)$.

3) The prediction is invariant with respect to a scaling of $P_{dep}^{(0)}$. Suppose the true value of $P_{dep}^{(0)}$ is not measurable. Instead, a quantity proportional to $P_{dep}^{(0)}$ with a fixed but unknown multiplier is measured. Let $Q = \alpha P_{dep}^{(0)}$ be the measured quantity where α is an unknown coefficient. For example, while it may be difficult to measure the power density deposited on the skin ($P_{dep}^{(0)}$), the power emitted at the antenna (Q) is proportional to $P_{dep}^{(0)}$ and is measured in experiments. The 3 data points with Q as the independent variable are at $Q = q_0, 2q_0$ and $4q_0$ where $q_0 = \alpha p_0$. Here q_0 is measured/specified but both α and p_0 are unknown. Let $\left(c_{2,Q}^{(est)}, c_{1,Q}^{(est)}, t_{del,Q}^{(est)}\right)$ be the solution of Equation (44) with Q as the independent variable. We have

$$c_{2,Q}^{(est)} = \alpha c_2^{(est)}, \quad c_{1,Q}^{(est)} = c_1^{(est)}, \quad t_{del,Q}^{(est)} = t_{del}^{(est)}$$

The predicted observed reflex time as a function of Q satisfies

$$t_{obs,Q}^{(pred)}(Q) = t_{obs}^{(pred)}\left(P_{dep}^{(0)}\right)$$

Therefore, for the purpose of determining t_{del}, we only need to measure $Q = \alpha P_{dep}^{(0)}$. There is no need to measure $P_{dep}^{(0)}$ or find the value of multiplier α.

It is worthwhile to point out that all of the properties above are attributed to the formulation form of (44). They are independent of the data on which algorithm (44) is applied. In particular, they are not affected by the true model governing the data generation in simulations or in experiments. Property 3 above is very powerful in applications. To estimate the time delay t_{del}, it is sufficient to measure i) the power emitted at the antenna (Q) and ii) the corresponding observed reflex time (t_{obs}). Both of these are readily measurable. In algorithm (44), using the measurable quantity Q as the independent variable instead of $P_{dep}^{(0)}$ does not introduce any additional error in estimating the time delay t_{del}. Formulation (44) is truly invariant with respect to scaling.

8.4. Energy Consumption vs. Applied Power

Let Q_{skin} be the power absorbed in the skin (energy absorbed per time) and $Q_{antenna}$ be the power emitted at the antenna of radiators. At a fixed beam radius w and at a fixed distance d between the antenna and the test subject, $Q_{antenna}$ is proportional to Q_{skin}, which in turn is proportional to $P_{dep}^{(0)}$, the power density absorbed in the skin at the beam center.

$$Q_{skin} = P_{dep}^{(0)} \int_0^{+\infty} 2\pi r \exp\left(-\frac{2r^2}{w^2}\right) dr = P_{dep}^{(0)} \cdot \frac{\pi w^2}{2}$$

$$Q_{antenna} = \beta(w,d) Q_{skin} = P_{dep}^{(0)} \cdot \frac{\pi w^2}{2} \beta(w,d)$$

The proportionality constant $\frac{\pi w^2}{2}\beta(w,d)$ is independent of $P_{\text{dep}}^{(0)}$.

Let E_{antenna} be the total energy emitted at the antenna by the time of withdrawal reflex t_{ref}. Energy E_{antenna} is proportional to $t_{\text{ref}}\left(P_{\text{dep}}^{(0)}\right)P_{\text{dep}}^{(0)}$

$$E_{\text{antenna}} = t_{\text{ref}}Q_{\text{antenna}} = t_{\text{ref}}\left(P_{\text{dep}}^{(0)}\right)P_{\text{dep}}^{(0)} \cdot \frac{\pi w^2}{2}\beta(w,d)$$

We treat E_{antenna} as the energy consumption and study it as a function of applied power density $P_{\text{dep}}^{(0)}$. Since the proportionality constant $\frac{\pi w^2}{2}\beta(w,d)$ is independent of $P_{\text{dep}}^{(0)}$, we use $t_{\text{ref}}\left(P_{\text{dep}}^{(0)}\right)P_{\text{dep}}^{(0)}$ as a measure of energy consumption. **Figure 11** plots $t_{\text{ref}}\left(P_{\text{dep}}^{(0)}\right)P_{\text{dep}}^{(0)}$ vs $P_{\text{dep}}^{(0)}$ for a Gaussian beam. In **Figure 11**, the energy consumption varies with the applied power density and it attains a minimum at a moderate value of $P_{\text{dep}}^{(0)}$.

In case B, we showed analytically (in subsection 7.4) that the energy consumption attains a minimum at an intermediate range of applied power density. The minimum energy consumption is attributed to the two opposite effects of heat conduction on temperature increase, respectively over short time and over long time. In case B, with a given beam spot area, withdrawal reflex occurs when the temperature at a fixed depth reaches the nociceptor activation temperature. Mathematically, we derived (in subsection 7.3) that at a fixed depth, over short time the net heat gain via conduction is positive. When the applied power is large, the reflex occurs in short time. Over that short time, the heat conduction augments the temperature increase of electromagnetic heating, speeds up the process of reaching the activation temperature, and reduces the energy consumption. In the regime of large applied power, increasing the applied power further makes the reflex time very short and leaves very little time for the conduction to take its effect in reducing the energy consumption. As a result, in the regime of large
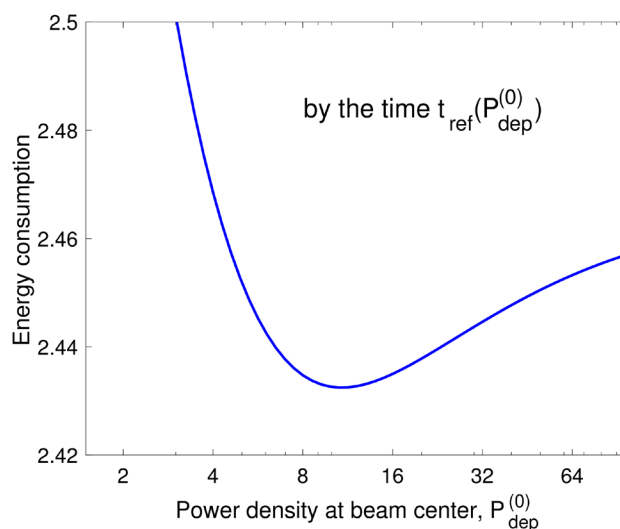

Figure 11. Energy consumption by the reflex time $t_{\text{ref}}\left(P_{\text{dep}}^{(0)}\right)$.

applied power, the energy consumption increases with the applied power. At a given depth, the positive net heat gain via conduction depends on the heat in-flow from upstream. At the skin surface, however, there is no heat in-flow. As time goes on, the effect of insulated boundary propagates in the depth direction in the form of attenuating the heat flow. Mathematically, at a fixed depth, eventually the net heat gain via conduction turns negative and the magnitude of net heat loss grows with time. When the applied power is small, it takes long time to induce the reflex. Over that long time, the heat conduction yields net heat loss, diminishes the temperature increase of electromagnetic heating, slows down the process of reaching the activation temperature, and drives up the energy consumption. In the regime of small applied power, reducing the applied power will give the conduction more time to take its effect in neutralizing the electromagnetic heating, and increase the energy consumption. Consequently, In the regime of small applied power, the energy consumption increases when the applied power is lowered. The transition between these two regimes produces a minimum for the energy consumption. Although the behaviors of these two regimes were derived for the idealized case B, in the case of a Gaussian beam, we observe the same behaviors in **Figure 11**: in the regime of small $P_{\text{dep}}^{(0)}$ when $P_{\text{dep}}^{(0)}$ increases, energy consumption is reduced; in the regime of large $P_{\text{dep}}^{(0)}$, energy consumption increases with $P_{\text{dep}}^{(0)}$; the transition between these two trends produce a minimum energy in the middle. **Figure 11** indicates that the two opposite effects of heat conduction on temperature increase, respectively over short time and over long time, are present in all situations even when the idealized conditions are not met.

Figure 11 describes the energy consumption in the situation where the power is turned off exactly at the predicted internal initiation of withdrawal reflex (before the actual occurrence of observed reflex). Given that the predicted $t_{\text{ref}}\left(P_{\text{dep}}^{(0)}\right)$ is not exact, to ensure that the applied beam induce the withdrawal reflex, it is prudent to keep the power on for a short time beyond $t_{\text{ref}}\left(P_{\text{dep}}^{(0)}\right)$. In real operations, adding a short time serves as a cushion for accommodating the uncertainty in estimating t_{del}. The uncertainty is in the form of an absolute error in the estimated t_{del}, which leads to an absolute error in the estimated true reflex time $t_{\text{ref}} = t_{\text{obs}} - t_{\text{del}}$. We study the energy consumption until (t_{ref} + cushion time), as a function of applied power density. **Figure 12** plots $\left(t_{\text{ref}}\left(P_{\text{dep}}^{(0)}\right)+0.05\right)P_{\text{dep}}^{(0)}$ vs $P_{\text{dep}}^{(0)}$. With a fixed short time 0.05 added to t_{ref}, the energy consumption has a more pronounced minimum, which also occurs at a more moderate range of applied power.

8.5. Determining $\left(T_{\text{act}}, z_c\right)$ from Test Data

In subsection 7.6, we discussed selecting test conditions for producing distinct constraint functions on $\left(T_{\text{act}}, z_c\right)$ in the idealized case B. We found that a combination of large beam spot area A_{nd} and moderate applied power density $P_{\text{dep,nd}}$ yields a flat T_{act} vs z_c while a combination of moderate A_{nd} and
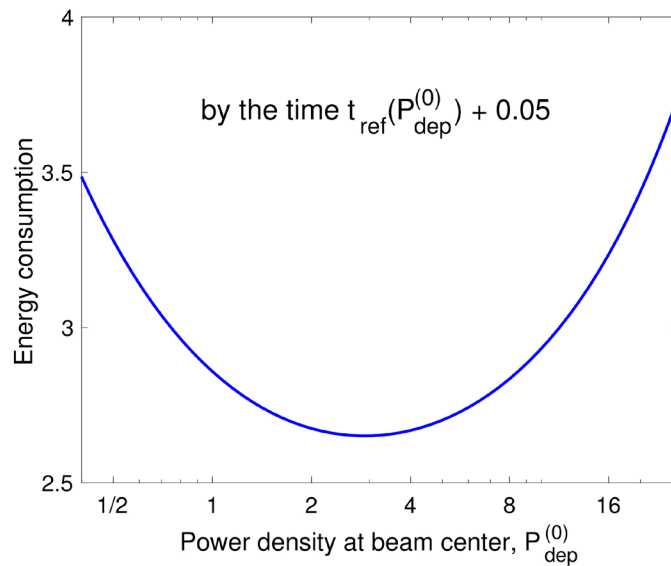
Figure 12. Energy consumption by the time $\left(t_{\text{ref}} \left(P_{\text{dep}}^{(0)} \right) + 0.05 \right)$.

large $P_{\text{dep,nd}}$ gives a slant T_{act} vs z_c. In this subsection, we test this strategy in the case of a Gaussian beam.

We use the temperature distribution given in (61). To mimic the situation of real applications, we work with $T(\boldsymbol{r}, y)$, the physical temperature in physical coordinates. In simulations of this subsection, we use

$$c_1 = 1, \quad c_2 = 1/2, \quad \mu = 1, \quad z_c^* = 1, \quad T_0 = 37, \quad T_{act}^* = 41$$

Here, for clarity, we reserve $\left(T_{\text{act}}^*, z_c^* \right)$ as the notation for the true value of $\left(T_{\text{act}}, z_c \right)$ and use the general notation $\left(T_{\text{act}}, z_c \right)$ to represent the variables in constraint functions. We run simulations using the parameters listed above with various combinations of $\left(w, P_{\text{dep}}^{(0)} \right)$ to generate simulated data sets. Each data set consists of the reflex time t_{ref} and the temperature distribution $T(\boldsymbol{r}, y, t)$ for a particular test condition $\left(w, P_{\text{dep}}^{(0)} \right)$. For each data set, we apply formulation (5) described in section 4 to construct a constraint function on $\left(T_{\text{act}}, z_c \right)$. Formulation (5) is based solely on the data of spatial temperature profile at reflex $T(\boldsymbol{r}, y, t_{\text{ref}})$. It does not require any input parameter. **Figure 13** displays constraint functions for 3 combinations of $\left(w, P_{\text{dep}}^{(0)} \right)$. It demonstrates the same behaviors as we observed in case B: increasing the beam radius w makes the constraint curve T_{act} vs z_c flat while decreasing w makes the curve slate. The intersection of distinct constraint curves gives us the true value $\left(T_{\text{act}}^*, z_c^* \right)$.

9. Concluding Remarks

We studied theoretically the occurrence of heat-induced withdrawal reflex caused by exposure to an electromagnetic beam. We investigated several aspects of the problem, including i) non-dimensionalization to pinpoint the effects of parameters; ii) normalization of the non-dimensional temperature into a parameter-free function; iii) forward prediction of system behaviors given model
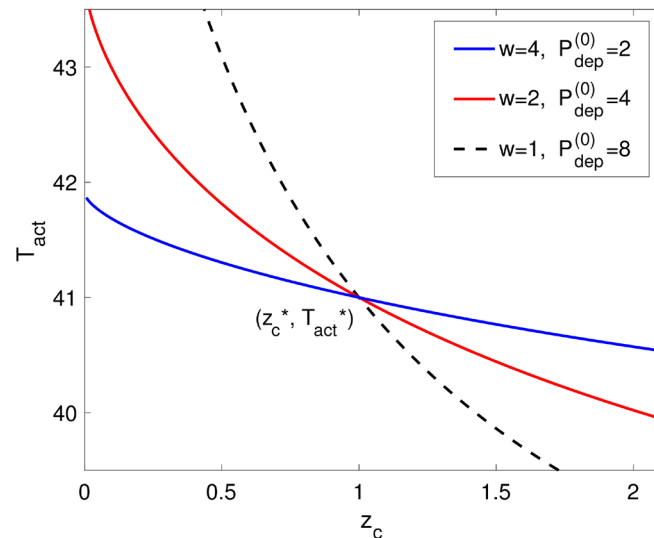
Figure 13. Constraint functions constructed from simulated data for a Gaussian beam. Three distinct constraint curves are shown, corresponding to three test conditions.

Parameters; iv) asymptotic behaviors in certain regimes of parameters; and v) backward inference of model parameters based on measured data.

First, we reviewed the model components used in ADT CHEETEH-E [17], and we synthesized them to distill a concise dose-response model for predicting the occurrence of withdrawal reflex based on the given spatial temperature profile. In the dose-response relation, the dose quantity is defined as the volume of the activated region of heat-sensitive nociceptors. Under the assumption that the nociceptor density is uniform in the skin, the activated volume is proportional to the total number of nociceptors activated, and thus, increases monotonically with the perceived pain level, which controls the occurrence of withdrawal reflex. In a deterministic setting, withdrawal reflex occurs precisely when the activated volume reaches a critical threshold. The resulting dose-response relation described in (4) is specified by two parameters: the nociceptor activation temperature T_{act} and the critical threshold z_c on the activated volume for withdrawal reflex.

The concise model has the advantage that the two parameters can be determined from test data in the situation where the reflex time and the spatial temperature profile at reflex are measurable. Parameters T_{act} and z_c are constrained by function (5), which is constructed solely from the measured temperature profile at reflex. The inference method based on (5) is parameter-free, requiring no input parameter. The data set measured at each test condition provides only one constraint on (T_{act}, z_c). To determine the two unknown parameters, several tests at various conditions are needed to produce distinct constraint functions. The intersection of distinct constraint curves yields the true value (T_{act}, z_c).

The dose-response relation predicts the occurrence of withdrawal reflex from the given spatial temperature profile. We connected it with a time evolution

model for the temperature increase of electromagnetic heating. The result is a composite model that takes as input the test condition described by two tunable quantities: the beam spot area and the applied power density. Other quantities, such as the initial temperature, the characteristic depth of the electromagnetic wave penetrating into the skin and the nociceptor activation temperature, are viewed as parameters. In the composite model, the time evolution model produces the temperature distribution from the test condition, and then the dose-response relation uses the temperature distribution to determine the time of withdrawal reflex. We solved the composite model analytically in two idealized cases, first in the case of no heat conduction and uniform electromagnetic heating over beam cross-section (case A).

To examine the validity of the no-conduction assumption, we investigated the effect of heat conduction on temperature distribution. In the case of uniform electromagnetic heating over beam cross-section with heat conduction in the depth direction (case B), we carried out non-dimensionalization to facilitate the exact solution and to pinpoint the effects of model parameters. We solved the non-dimensional system analytically to obtain the exact solution given in (22). As a function of non-dimensional time and depth, the non-dimensional temperature is the product of the non-dimensional power density and a parameter-free function, which is called the normalized temperature. The normalized temperature has no dependence on the power density or any other parameters. The effects of physical parameters are contained in the non-dimensional variables and quantities. Scaling temperature distribution into a parameter-free function significantly simplifies the structure of exact solution and reveals its dependence on parameters. We compared the normalized temperatures in the presence and in the absence of heat conduction. We found that the no-conduction approximation is valid only in the region away from the skin surface and only over a short time. Both conditions need to be satisfied in order to make the effect of heat conduction negligible. This result indicates that the no-conduction approximation is not an adequate tool for analyzing the temperature evolution near the skin surface.

Using the exact solution obtained in case B (the case with heat conduction), we studied theoretical behaviors of the system. Below are the findings.

- As the beam spot area A increases, the reflex time decreases rapidly to a positive value above zero. The convergence is described by $1/A^2$ in (34).
- We define the true reflex time as the moment when the number of activated nociceptors is sufficiently large to produce a perceived pain level exceeding the tolerance and thus to initiate the withdrawal reflex. The observed reflex time is when the reflex response (*i.e.*, the subject moving out of the beam) actually takes place. There is a latency (time delay) between the observed reflex time and the true reflex time. We assume that the latency is intrinsic to the subject being tested and is independent of the applied power density. We derived algorithm (44) for inferring the time delay from measured values of

observed reflex times at a sequence of applied power density values. Once the time delay is obtained, the true reflex time is calculated from the observed reflex time.

- The true reflex time decreases when the applied power density is increased. To examine the behaviors respectively at large and at small applied power density, we carried out asymptotic expansions of the normalized temperature respectively for small and large time. From the expansions of the normalized temperature, we derived asymptotic approximations of the reflex time, respectively, for large applied power density given in (51) and for small power density given in (52). At a fixed beam spot area, the product of beam power density and reflex time is proportional to the energy consumed for inducing withdrawal reflex. The asymptotic analysis indicates that when we increase the power density gradually in the small regime, initially the energy consumption decreases and then it attains a minimum; eventually in the large regime, further increase of power density leads to an increase in energy consumption. The two sides of the energy consumption curve surrounding the minimum correspond to the two opposite effects of heat conduction, respectively over short time and over long time. At a fixed depth, over short time, heat conduction augments the temperature increase of electromagnetic heating. It leads to a temperature growth faster than the no-conduction solution and reduces the energy consumption by shortening the reflex time. In contrast, over long time, heat conduction diminishes the temperature increase of electromagnetic heating. It results in a much slower temperature growth than the no-conduction solution and drives up the energy consumption needed for inducing withdrawal reflex.

- We examined the spatial temperature profile at reflex and how it varies with the applied power density. We found that at a fixed depth, for large power density, the temperature at reflex converges to the no-conduction solution. This result indicates that it is appropriate to neglect the effect of heat conduction only when the location is away from the skin surface and when the (non-dimensional) power density is large.

- In the situation where the spatial temperature profile at reflex is measured in tests, we studied the methodology for determining $\left(T_{\mathrm{act}}, z_c\right)$ from test data. $\left(T_{\mathrm{act}}, z_c\right)$ is constrained by Equation (5), which is parameter-free and is constructed based solely on the measured spatial temperature profile. The intersection of two or more distinct constraint curves, calculated from test data at various test conditions, determines the true value $\left(T_{\mathrm{act}}, z_c\right)$. We explored how to select test conditions to produce significantly distinct constraints on $\left(T_{\mathrm{act}}, z_c\right)$. We found that the steepness of $T_{\mathrm{act}}\left(z_c\right)$ is negatively associated with the beam spot area. For the purpose of estimating $\left(T_{\mathrm{act}}, z_c\right)$, we need to carry out tests with moderate beam spot area and with large beam spot area. This is to ensure that the constraint curves constructed from test data are substantially distinct and have a well-defined intersection.

We conducted a case study of a Gaussian beam with finite beam radius and with heat conduction in the depth direction. Since it has no closed-form solution, the case study was carried out using numerical simulations. The goal was to test the theoretical results predicted for the idealized case of uniform temperature over beam cross-section (case B). We first examined the performance of algorithm (44) for determining the unknown latency from measured values of observed reflex times at a sequence of applied power density values. Algorithm (44) was derived under the assumptions of case B and in the limit of beam spot area approaching infinity. (44) calculates the time delay solely from 3 data points of $\left(P_{\text{dep}}, t_{\text{obs}}\right)$ where P_{dep} is the applied power density and t_{obs} is the corresponding observed reflex time. Algorithm (44) does not require any input parameter. Operationally, it is universally applicable in all situations where the observed reflex time is measured. We applied it to the case of a Gaussian beam with a finite beam radius. In Figure 10, the estimated time delay is very close to the true value, suggesting the wide applicability of algorithm (44) beyond the idealized case B.

In addition to its high accuracy, formulation (44) has an important scaling property: the prediction by (44) is invariant with respect to a scaling in the independent variable P_{dep}. At a fixed beam radius and fixed distance from the test subject, the power emitted at the antenna is proportional to the beam center power density. The scaling property allows us to use the power emitted at the antenna as the independent variable in (44). The calculation of t_{del} in (44) is independent of the proportionality constant in scaling. The time delay calculated this way will be the same as if we use the beam center power density as the independent variable in (44). This scaling property is especially useful when it is impractical to measure the beam center power density deposited on the skin.

In the case of a Gaussian beam, we examined numerically the energy consumption for inducing withdrawal reflex as a function of applied power density. We first considered the situation where the power is turned off at the true reflex time when the activated volume reaches the threshold to start the internal initiation of withdrawal reflex. The observed reflex action (the subject moving out of beam) occurs with time delay t_{del} after the internal initiation. We observed that a minimum energy consumption is attained at a moderately large beam center power density, similar to what we theoretically predicted in the idealized case B. This observation suggests that the existence of minimum energy consumption may be a general phenomenon in all situations. In the situation where we keep the power on for a short period beyond the true reflex time, the energy consumption has a more pronounced minimum, which is attained at a more moderate value of the applied power density.

In the case of a Gaussian beam, we tested the strategy of selecting test conditions for determining parameters T_{act} and z_c. Again, the theoretical behavior of constraint function $T_{\text{act}}\left(z_c\right)$, established in the idealized case B, remains qualitatively true for a Gaussian beam: the slope of constraint function $T_{\text{act}}\left(z_c\right)$

decreases when the beam size is increased. To obtain substantially distinct constraint curves for (T_{act}, z_c), we need to carry out tests with a moderate beam radius and with a large beam radius.

In summary, in a deterministic setting, we studied mathematically the system from the electromagnetic power deposited on the subject's skin to the subject's behavioral response. Our theoretical findings provide insight into how the system behaves in various regimes of model parameters and how the system behavior varies in response to changes in parameters. Furthermore, through theoretical formulation and analysis in idealized cases, we established a mathematical framework for designing tunable parameters in tests to fully sample the effects of hidden parameters in test data. Properly sampling the effects of model parameters in test data is a vital step toward reliably determining the values of these parameters.

Acknowledgements and Disclaimer

Conflicts of Interest

The authors declare no conflicts of interest regarding the publication of this paper.

References

[1] Romanenko, S., Siegel, P.H., Wagenaar, D.A. and Pikov, V. (2014) Effects of Millimeter Wave Irradiation and Equivalent Thermal Heating of Individual Neurons in the Leech Ganglion. *Journal of Neurophysiology*, **112**, 2423-2413. https://doi.org/10.1152/jn.00357.2014

[2] Topfer, F. and Oberhammer, J. (2015) Millimeter-Wave Tissue Diagnosis: The Most Promising Fields for Medical Applications. *IEEE Microwave Magazine*, **16**, 97-113. https://doi.org/10.1109/MMM.2015.2394020

[3] Kuutti, J., Paukkunen, M., Aalto, M., Eskelinen, P. and Sepponen, R.E. (2015) Evaluation of a Doppler Radar Sensor System for Vital Signs Detection and Activity Monitoring in a Radio-Frequency Shielded Room. *Measurement*, **68**, 135-142. https://doi.org/10.1016/j.measurement.2015.02.048

[4] Zhadobov, M., Chahat, N., Sauleau, R., Le Quement, C. and Le Drean, Y. (2011) Millimeter-Wave Interactions with the Human Body: State of Knowledge and Recent Advances. *International Journal of Microwave and Wireless Technologies*, **3**, 237-247. https://doi.org/10.1017/S1759078711000122

[5] Walters, T.J., Blick, D.W., Johnson, L.R., Adair, E.R. and Foster, K.R. (2000) Heating and Pain Sensation Produced in Human Skin by Millimeter Waves: Comparison

to a Simple Thermal Model. *Health Physics*, **78**, 259-267.
https://doi.org/10.1097/00004032-200003000-00003

[6] Foster, K.R., Lozano-Nieto, A. and Riu, P. (1998) Heating of Tissues by Microwaves: A Model Analysis. *Bioelectromagnetics*, **19**, 420-428.
https://doi.org/10.1002/(SICI)1521-186X(1998)19:7<420::AID-BEM3>3.0.CO;2-3

[7] Ozen, S., Helhel, S. and Cerezci, O. (2008) Heat Analysis of Biological Tissue Exposed to Microwave by Using Thermal Wave Model of Bio-Heat Transfer (TWMBT). *Burns*, **34**, 45-49. https://doi.org/10.1016/j.burns.2007.01.009

[8] Ozen, S., Helhel, S. and Bilgin, S. (2011) Temperature and Burn Injury Prediction of Human Skin Exposed to Microwaves: A Model Analysis. *Radiation and Environmental Biophysics*, **50**, 483-489. https://doi.org/10.1007/s00411-011-0364-y

[9] Nelson, D.A., Nelson, M.T., Walters, T.J. and Mason, P.A. (2000) Skin Heating Effects of Millimeter-Wave Irradiation—Thermal Modeling Results. *IEEE Transactions on Microwave Theory and Techniques*, **48**, 2111-2120.
https://doi.org/10.1109/22.884202

[10] Laakso, I., Morimoto, R., Heinonen, J., Jokela, K. and Hirata, A. (2017) Human Exposure to Pulsed Fields in the Frequency Range from 6 to 100 GHz. *Physics in Medicine & Biology*, **62**, 6980-6992. https://doi.org/10.1088/1361-6560/aa81fe

[11] Foster, K.R., Ziskin, M.C. and Balzano, Q. (2016) Thermal Response of Human Skin to Microwave Energy: A Critical Review. *Health Physics*, **111**, 528-541.
https://doi.org/10.1097/HP.0000000000000571

[12] Ryan, K.L., D'Andrea, J.A., Jauchem, J.R. and Mason, P.A. (2000) Radio Frequency Radiation of Millimeter Wave Length: Potential Occupational Safety Issues Relating to Surface Heating. *Health Physics*, **78**, 170-181.
https://doi.org/10.1097/00004032-200002000-00006

[13] Parker, J.E., Nelson, E.J., Beason, C.W. and Cook, M.C. (2017) Thermal and Behavioral Effects of Exposure to 30 Kw, 95-GHz Millimeter Wave Energy. Technical Report, AFRL-RH-FS-TR-2017-0016.

[14] Parker, J.E., Nelson, E.J., Beason, C.W. and Cook, M.C. (2017) Effects of Variable Spot Size on Human Exposure to 95-GHz Millimeter Wave Energy. Technical Report, AFRL-RH-FS-TQ-2017-0017.

[15] Plaghki, L., Decruynaere, C., Van Dooren, P. and Le Bars, D. (2010) The Fine Tuning of Pain Thresholds: A Sophisticated Double Alarm System. *PLoS ONE*, **5**, e10269. https://doi.org/10.1371/journal.pone.0010269

[16] Martin, E. and Hine, R. (2015) A Dictionary of Biology. 7th Edition, Oxford University Press, Oxford.

[17] Cazares, S.M., Snyder, J.A., Belanich, J., Biddle, J.C., Buytendyk, A.M., Teng, S.H.M. and O'Connor, K. (2019) Active Denial Technology Computational Human Effects End-to-End Hypermodel for Effectiveness (ADT CHEETEH-E). Institute for Defense Analyses. IDA Document NS D-10435.
https://doi.org/10.1007/s41314-019-0023-7

Appendix A: Exact Solution of Case A

In case A defined in (9), the temperature distribution $T(\boldsymbol{r}, y, t)$ is governed by

$$
\begin{cases}
\rho C_p \dfrac{\partial T(\boldsymbol{r}, y, t)}{\partial t} = P_{\mathrm{dep}} \mu \mathrm{e}^{-\mu y}, & \text{for } \boldsymbol{r} \in A \\
T(\boldsymbol{r}, y, 0) = T_0
\end{cases}
$$

Integrating with respect to *t* yields the temperature distribution

$$
T(\boldsymbol{r}, y, t) = T_0 + t \frac{P_{\mathrm{dep}} \mu}{\rho C_p} \mathrm{e}^{-\mu y}, \quad \text{for } \boldsymbol{r} \in A \tag{65}
$$

Since case A is a special situation of case U, the reflex time t_{ref} is governed by Equation (8). With the expression of $T(y, t)$ given in (65), equation for t_{ref} becomes

$$
T_0 + t_{\mathrm{ref}} \frac{P_{\mathrm{dep}} \mu}{\rho C_p} \mathrm{e}^{-\mu z_c / A} = T_{\mathrm{act}}
$$

Solving for t_{ref}, we obtain

$$
t_{\mathrm{ref}} = \frac{T_{\mathrm{act}} - T_0}{P_{\mathrm{dep}}} \cdot \frac{\rho C_p}{\mu} \mathrm{e}^{\mu z_c / A} \tag{2}
$$

Appendix B: Analytic Expression of Function $G(y, t)$

Recall that $G(y, t)$ is defined as the solution of

$$
\begin{cases}
\dfrac{\partial G}{\partial t} = \dfrac{\partial^2 G}{\partial y^2} \\
\left. \dfrac{\partial G}{\partial y} \right|_{y=0} = 0, \quad G(y, 0) = \mathrm{e}^{-y}
\end{cases}
$$

To solve for $G(y, t)$, we first convert the initial boundary value problem to an initial value problem by extending the initial condition for $y \geq 0$ to an even function of *y*.

$$
\begin{cases}
\dfrac{\partial G}{\partial t} = \dfrac{\partial^2 G}{\partial y^2} \\
G(y, 0) = \mathrm{e}^{-|y|}
\end{cases}
$$

Using the fundamental solution of the heat equation, we write $G(y, t)$ as

$$
\begin{aligned}
G(y, t) &= \int_{-\infty}^{+\infty} \frac{\mathrm{e}^{-(y-u)^2 / (4t)}}{\sqrt{4\pi t}} \mathrm{e}^{-|u|} \mathrm{d}u \\
&= \int_0^{+\infty} \frac{\mathrm{e}^{-(y-u)^2 / (4t)}}{\sqrt{4\pi t}} \mathrm{e}^{-u} \mathrm{d}u + \int_0^{+\infty} \frac{\mathrm{e}^{-(u+y)^2 / (4t)}}{\sqrt{4\pi t}} \mathrm{e}^{-u} \mathrm{d}u \\
&\equiv I_1 + I_2
\end{aligned}
$$

Completing the square in the exponent of term I_1, we get

$$I_1 = \int_0^{+\infty} \frac{1}{\sqrt{4\pi t}} \exp\left(-\left[\frac{u+2t-y}{\sqrt{4t}}\right]^2\right) du \cdot \exp(t-y)$$

$$= \int_{\frac{2t-y}{\sqrt{4t}}}^{+\infty} \frac{1}{\sqrt{\pi}} \exp(-w^2) dw \cdot e^{t-y}$$

$$= \frac{1}{2} \mathrm{erfc}\left(\frac{2t-y}{\sqrt{4t}}\right) \cdot e^{t-y}$$

Similarly, we can derive

$$I_2 = \frac{1}{2} \mathrm{erfc}\left(\frac{2t+y}{\sqrt{4t}}\right) \cdot e^{t+y}$$

Substituting I_1 and I_2 into the expression of $G(y,t)$, we arrive at

$$G(y,t) = \frac{1}{2} \mathrm{erfc}\left(\frac{2t-y}{\sqrt{4t}}\right) e^{t-y} + \frac{1}{2} \mathrm{erfc}\left(\frac{2t+y}{\sqrt{4t}}\right) e^{t+y} \qquad (67)$$

Appendix C: Asymptotics of Functions $h(t)$, $h^{-1}(u)$ and $R(u)$

Recall that function $R(u)$ is defined in (42) in terms of $h^{-1}(u)$. Function $h(t)$ is

$$h(t) \equiv \int_0^t \mathrm{erfc}(\sqrt{s}) e^s ds = \mathrm{erfc}(\sqrt{t}) e^t - 1 + \frac{2}{\sqrt{\pi}}\sqrt{t}$$

We carry out analysis in steps below to derive the asymptotics of $R(u)$.

Step 1: We first show that $h^{-1}(u)$ is well defined. We show that for $t \in [0,+\infty)$, function $h(t)$ increases with t, and its range is $[0,+\infty)$.

Noticing that $h(0)=0$ and $h'(t) = \mathrm{erfc}(\sqrt{t}) e^t > 0$. To prove that the range of $h(t)$ is $[0,+\infty)$, we derive the asymptotic of $h(t)$ for large t. We write $h(t)$ as

$$h(t) = \mathrm{erfcx}(z)\big|_{z=\sqrt{t}} - 1 + \frac{2}{\sqrt{\pi}}\sqrt{t}$$

where $\mathrm{erfcx}(z)$ is the scaled complementary error function and has the expansion

$$\mathrm{erfcx}(z) \equiv \mathrm{erfc}(z) \exp(z^2)$$
$$= \frac{1}{\sqrt{\pi} z}\left(1 - \frac{1}{2z^2} + \frac{3}{4z^4} - \frac{15}{8z^6} + \cdots\right) \text{ for large } z \qquad (68)$$

Using (68), we write out the expansion of $h(t)$ for large t

$$h(t) = \frac{2}{\sqrt{\pi}}\sqrt{t}\left(1 - \frac{\sqrt{\pi}}{2\sqrt{t}} + \frac{1}{2t} + \cdots\right) \text{ for large } t \qquad (69)$$

As t goes to infinity, $h(t)$ increases unbounded. Thus, the range of $h(t)$ is $[0,+\infty)$.

Step 2: Using the results of $h(t)$ obtained in Step 1, we see that $h^{-1}(u)$ is well defined for $u \in [0,+\infty)$. In this step, we derive the expansion of $h^{-1}(u)$

for large *u*.

We notice that *u* as a function of $t \equiv h^{-1}(u)$ has the expansion given in (69).

$$u = h(t) = \frac{2}{\sqrt{\pi}}\sqrt{t}\left(1 - \frac{\sqrt{\pi}}{2\sqrt{t}} + \frac{1}{2t} + \cdots\right)$$

Based on this, we write out an iterative formula for expanding $t = h^{-1}(u)$

$$\sqrt{t^{(k+1)}} = \frac{\sqrt{\pi}}{2}u\frac{1}{\left(1 - \frac{\sqrt{\pi}}{2\sqrt{t^{(k)}}} + \frac{1}{2t^{(k)}} + \cdots\right)}$$

Starting the iteration with $t^{(0)} = \infty$, we calculate $\sqrt{t^{(1)}}$, $\sqrt{t^{(2)}}$ and

$$\sqrt{t^{(3)}} = \frac{\sqrt{\pi}}{2}u\left(1 + \frac{1}{u} - \frac{2}{\pi}\frac{1}{u^2}\right)$$

Squaring both sides, we obtain the expansion of $t \equiv h^{-1}(u)$ as a function of *u*.

$$h^{-1}(u) = \frac{\pi}{4}\left[u^2 + 2u + \left(1 - \frac{4}{\pi}\right) + \cdots\right] \quad \text{for large } u \tag{70}$$

Step 3: In this step, we expand $R(u)$ for large *u*. Using (6), we write

$$h^{-1}(u) - h^{-1}(u/2) = \frac{\pi}{4}\left[\frac{3}{4}u^2 + u + O\left(\frac{1}{u}\right) + \cdots\right]$$

$$R(u) = \frac{\left(h^{-1}(u) - h^{-1}(u/2)\right) - 2\left(h^{-1}(u/2) - h^{-1}(u/4)\right)}{\left(h^{-1}(u) - h^{-1}(u/2)\right) + 2\left(h^{-1}(u/2) - h^{-1}(u/4)\right)}$$

$$= \frac{1}{3}\left[1 - \frac{16}{9u} + \frac{16^2}{9^2 u^2} + O\left(\frac{1}{u^3}\right)\right] \quad \text{for large } u \tag{71}$$

Step 4: In this step, we expand $h^{-1}(u)$ for small *u*. We start with the expansion of $h(t)$

$$h(t) = \text{erfc}\left(\sqrt{t}\right)e^t - 1 + \frac{2}{\sqrt{\pi}}\sqrt{t}$$

$$= t\left(1 - \frac{4}{3\sqrt{\pi}}t^{1/2} + \frac{1}{2}t + O\left(t^{3/2}\right)\right) \quad \text{for small } t \tag{72}$$

Based on this, we write out an iterative formula for expanding $t = h^{-1}(u)$

$$t^{(k+1)} = \frac{u}{\left(1 - \frac{4}{3\sqrt{\pi}}\sqrt{t^{(k)}} + \frac{1}{2}t^{(k)} + \cdots\right)}$$

Starting the iteration with $t^{(0)} = 0$, we calculate $t^{(1)}$, $t^{(2)}$, and

$$t^{(3)} = u\left(1 + \frac{4}{3\sqrt{\pi}}\sqrt{u} + \left(\frac{8}{3\pi} - \frac{1}{2}\right)u\right)$$

Thus, near $u = 0$ function $h^{-1}(u)$ has the expansion

$$h^{-1}(u) = u + \frac{4}{3\sqrt{\pi}}u^{3/2} + \left(\frac{8}{3\pi} - \frac{1}{2}\right)u^2 + \cdots \quad \text{for small } u \tag{73}$$

Step 5: In this step, we expand $R(u)$ for small u. Using (73), we write

$$h^{-1}(u) - h^{-1}(u/2) = \frac{1}{2}u + \left(1 - \frac{1}{2\sqrt{2}}\right)\frac{4}{3\sqrt{\pi}}u^{3/2} + \left(\frac{2}{\pi} - \frac{3}{8}\right)u^2 + \cdots$$

$$\begin{aligned} R(u) &= \frac{\left(h^{-1}(u) - h^{-1}(u/2)\right) - 2\left(h^{-1}(u/2) - h^{-1}(u/4)\right)}{\left(h^{-1}(u) - h^{-1}(u/2)\right) + 2\left(h^{-1}(u/2) - h^{-1}(u/4)\right)} \\ &= \frac{5 - 3\sqrt{2}}{3\sqrt{\pi}}u^{1/2} + \left(\frac{4\sqrt{2}}{9\pi} - \frac{3}{16}\right)u + \cdots \quad \text{for small } u \end{aligned} \tag{74}$$

Appendix D: Calculation of $c_0(y)$ in Expansion (47)

The expansion of $H(y,t)$ for large t is given in (47) with $c_0(y)$ undetermined. Recall that $H(y,t)$ is governed by Equation (20). To derive $c_0(y)$, we substituting expansion (47) into (20). The balance of leading terms gives us $c_0''(y) + e^{-y} = 0$, which leads to

$$c_0(y) = -e^{-y} + a_0 + a_1 y$$

The insulated boundary condition $\left(\partial H/\partial y\right)\big|_{y=0} = 0$ yields $a_1 = -1$. To determine a_0, we compare the expansion of $H(0,t)$ for large t given in (69) with expansion (47) at $y = 0$. We obtain $a_0 = 0$. Thus, $c_0(y)$ in expansion (47) has the expression

$$c_0(h) = -\left(e^{-y} + y\right).$$